NACA

RESEARCH MEMORANDUM

EFFECT OF ICE FORMATIONS ON SECTION DRAG OF SWEPT NACA

63A-009 AIRFOIL WITH PARTIAL-SPAN LEADING-EDGE SLAT

FOR VARIOUS MODES OF THERMAL ICE PROTECTION

By Uwe H. von Glahn and Vernon H. Gray

Lewis Flight Propulsion Laboratory
Cleveland, Ohio

NATIONAL ADVISORY COMMITTEE
FOR AERONAUTICS

WASHINGTON
March 15, 1954

NATIONAL ADVISORY COMMITTEE FOR AERONAUTICS

RESEARCH MEMORANDUM

EFFECT OF ICE FORMATIONS ON SECTION DRAG OF SWEPT NACA

63A-009 AIRFOIL WITH PARTIAL-SPAN LEADING-EDGE SLAT

FOR VARIOUS MODES OF THERMAL ICE PROTECTION

By Uwe H. von Glahn and Vernon H. Gray

SUMMARY

The effects of primary and runback ice formations on the section drag of a 36° swept NACA 63A-009 airfoil section with a partial-span leading-edge slat were studied over a range of angles of attack from 2° to 8° and airspeeds up to 260 miles per hour for icing conditions with liquid-water contents ranging from 0.39 to 1.23 grams per cubic meter and datum air temperatures from 10° to 25° F.

The results with slat retracted showed that glaze-ice formations caused large and rapid increases in section drag coefficient and that the rate of change in section drag coefficient for the swept 63A-009 airfoil was about $2\frac{1}{2}$ times that for an unswept 65_1-212 airfoil. Removal of the primary ice formations by cyclic de-icing caused the drag to return almost to the bare-airfoil drag value. A comprehensive study of the slat icing and de-icing characteristics was prevented by limitations of the heating system and wake interference caused by the slat tracks and hot-gas supply duct to the slat. In general, the studies showed that icing on a thin swept airfoil will result in more detrimental aerodynamic characteristics than on a thick unswept airfoil.

INTRODUCTION

As part of a comprehensive program to determine the effects of various ice formations on the aerodynamic characteristics of airfoils and to aid in the determination of design requirements for icing-protection systems, the NACA Lewis laboratory is conducting studies on the drag associated with icing of various airfoils. The initial study (ref. 1) considered the section drag characteristics in icing conditions of an NACA 65_1-212 airfoil with leading-edge section unheated, continuously heated, and intermittently heated for cyclic de-icing. This study included the effects of both primary ice formations and runback icing on the airfoil section drag, and also the effect of various frost formations

on the airfoil surfaces. The results showed that glaze-ice formations, either primary or runback, on the upper airfoil surface near the leading edge caused large and rapid increases in drag, especially at datum air temperatures approaching 32° F, whereas rime ice incurred at lower air temperatures did not appreciably affect the section drag coefficient. These results were obtained with a straight (unswept) airfoil section.

Modern high-speed aircraft frequently have sweptback wings and high-lift devices such as leading-edge slats; it is important, therefore, to investigate such airfoils in icing clouds to determine the differences in icing and aerodynamic characteristics, if any, between these and conventional unswept airfoils. It is desirable to evaluate the effect of sweepback on the shape of the leading-edge ice formations and the associated drag penalties, and compare the icing and drag characteristics of a slatted airfoil section with those of an unslatted section. Drag penalties caused by runback and residual ice formations associated with thermal protection systems utilizing various modes of heating should also be determined for both slatted and unslatted swept airfoils. With a thermal ice-protection system employing intermittent heating (cyclic de-icing), an ice-free spanwise parting strip located near the stagnation region facilitates ice removal from unswept airfoils (refs. 2 to 4). It is desirable, therefore, to compare the drag characteristics of a swept airfoil with and without such a parting strip.

The NACA Lewis laboratory has conducted a study of the drag characteristics in icing conditions of a swept, slatted-leading-edge airfoil model furnished by an aircraft manufacturer. This airfoil model was the first of its type under development to be equipped with a thermal cyclic de-icing system. The purpose of this study was to determine the problems associated with icing of this type of airfoil and to measure the section drag losses incurred with ice formations typical of various modes of heating. The model consisted of a 36° swept NACA 63A-009 airfoil section incorporating a slatted leading edge over only a portion of span in order to compare simultaneously the icing characteristics of the slatted section with those of the unslatted airfoil. The model was equipped with an icing-protection system utilizing a combination of electric and hot-gas heating systems and was operated both continuously and cyclically over a range of icing conditions. Because of model deficiencies that will be discussed later, only limited data were obtained for the effect on drag of ice formations on the slatted portion of the airfoil when the slat was extended. Primarily, the present report is an extension of reference 1 to include the drag characteristics of a swept airfoil in icing conditions.

APPARATUS AND INSTRUMENTATION

The model used in this study (fig. 1) is an NACA 63A-009 airfoil section of 6.9-foot chord in the streamwise direction and spanning the 6-foot height of the icing research tunnel. The leading and trailing edges of the model are sweptback at an angle of 36°. The airfoil leading-edge section consists of two main units, an unslatted or standard-airfoil section of approximately 28 inches spanwise extent and a movable slatted leading-edge section (fig. 2). (Herein, spanwise denotes a direction parallel to the leading edge.) The leading-edge slat is of 20-inch chord in the streamwise direction and 44 inches in spanwise extent. The slat moves forward on tracks and rollers into the air stream in a direction normal to the leading edge. A hydraulic system is utilized to move and hold the slat in any desired forward position. The slat tracks are curved so that the extended slat moves on a circular arc to positions forward of and below the lower surface of the rest of the airfoil section. The radius of curvature of the tracks is approximately 34 inches, and the full movement for the slat is over a 16° center angle.

Heating Systems

The slat leading edge was provided with an electrically heated ice-free parting strip consisting of a heating element secured to a spanwise fin which in turn was riveted to the airfoil skin at the stagnation region for normal cruise angle of attack. Electric heating elements were also secured around the periphery of the closing ribs at the spanwise ends of the slat. The upper and lower surfaces of the slat were gas-heated. Hot gas was introduced by means of a flexible tube into a D-duct running spanwise near the leading-edge region of the slat (fig. 2). The hot gas was distributed to both ends of the slat, then passed through a double-skin configuration in the upper slat surface, and exhausted into the center of the slat through small orifices. The lower surface of the slat near the D-duct baffle was heated by conduction from the baffle and by the exhaust gas from the upper skin. In addition, a series of six holes in the D-duct supplied supplemental hot gas to the lower surface. A portion of the rear face of the slat (slat surface contacting fixed airfoil when slat is retracted) was provided with a double skin to increase the heat-transfer characteristics. The trailing lip of the lower surface was heated by an extension of this double-skin configuration. The slat tracks were heated by electric heating elements secured along both sides of the tracks.

The fixed airfoil section behind the slat (downstream) was divided into four heating zones because of the location of the two slat tracks and the flexible hot-gas duct to the slat. Each zone was gas-heated by means of a supply duct from a common header, a spanwise D-duct, and a

chordwise double-skin configuration. Electric heating elements were used in each zone to obtain an ice-free parting strip near the normal cruise stagnation region of this airfoil section when the slat was extended.

The leading-edge region of the standard-airfoil section (unslatted), which constituted the portion of the model near the tunnel floor, was supplied with a gas-heated parting strip in the form of a small circular duct secured to a fin, which in turn was riveted to the skin at the normal cruise stagnation region (fig. 2). The upper and lower surfaces were gas-heated by means of a double-skin configuration for which the hot gas was supplied through a spanwise D-duct. The closing rib sections of the airfoil were electrically heated by elements secured along the ribs.

The airfoil section between the slat and the top of the tunnel was gas-heated by means of a double-skin configuration. The section imme-diately aft of the heatable leading-edge sections containing the electric leads and gas supply lines was heated by exhausting hot gas into the entire chamber. The aft portion of the model was steam-heated and oper-ated at a pressure slightly below free-stream static pressure to prevent leakage into the wake behind the airfoil. All leading-edge sections of the model were capable of being heated independently for cyclic ice removal or collectively for continuous heating.

Cycling of the hot gas was accomplished by the use of double-throated valves with two butterfly plates displaced 90° on a common shaft. The valves were pneumatically operated and controlled by solenoids.

Instrumentation

Two pressure rakes located 28 inches behind the trailing edge of the airfoil were used to measure the airfoil section drag. One rake, located 2 feet from the tunnel ceiling, measured the drag of the slatted-airfoil section; and the second rake, mounted 18 inches above the tunnel floor, measured the drag of the standard-airfoil section. The rakes each consisted of 80 electrically heated total-pressure tubes and five static-pressure tubes. The total-pressure tubes were spaced on 1/4-inch centers, and the static tubes were evenly distributed along the span of each rake slightly above the total-pressure tubes. The supports for the rake were gas-heated for icing protection.

EXPERIMENTAL CONDITIONS AND TECHNIQUES

The airfoil-section drag studies reported herein include the effect of ice formations on an unheated airfoil, the effect of primary and runback ice formations on an airfoil utilizing a cyclic de-icing system, and the effect of various amounts of runback icing on an airfoil with a continuous heating system that does not evaporate all the impinging water. The heating requirements necessary for adequate icing protection for this model were determined from a previous unpublished study. Changes in these heating quantities were made, when required, in order to obtain specific types of ice formations on the airfoil surfaces. For all studies, the full-span gas-heated compartment aft of the leading-edge section and the steam-heated aft portion of the model were heated as a unit to prevent frost formations.

The range of conditions studied in this evaluation was as follows: airspeed, 175 and 260 miles per hour; liquid-water content, 0.39 to 1.23 grams per cubic meter; and datum air temperature, 10° to 25° F. The geometric angle of attack of the airfoil was varied from 2^O to 8° with the slat fully retracted. With the slat extended 8° (half of maximum travel), the angle of attack for the airfoil was set at 6°. A special study was made at an angle of attack of 8° with slat half extended (8°) and fully extended (16°). In addition, ice formations were allowed to build up on the leading-edge sections at low angles of attack (2^O and 4°) for a period of about 4 minutes, and the angle then changed to 7° or 8°. This procedure permitted a measurement of the drag produced by icing that might be encountered with a cyclic de-icing system during a heat-off period for an airplane letting down through an icing cloud and then flaring out for a landing approach.

Datum-air temperature is defined and determined as the average surface temperature of the unheated leading-edge section. In icing conditions, the datum temperature was determined from thermocouples shielded from or not subject to the release of the heat of fusion from the impinging water droplets. For the range of conditions investigated, little difference between total and datum air temperature was found. The liquid-water content was determined from a previous calibration of the tunnel.

In the absence of exact knowledge of the droplet impingement characteristics of the test airfoil, the data are discussed in general terms of water catch, defined as a function only of liquid-water content and airspeed (ref. 1). By this means, the size of the ice formations obtained at the airspeeds and liquid-water contents used in this study may be assumed, for example, to be approximately representative of ice formations that would be obtained at twice the airspeed and half the liquid-water content.

Throughout the study, photographs of the ice formations on the air-
foil surfaces were made to correlate the size and shape of these forma-
tions with the changes in drag as determined with the wake rakes (ref.
5). These changes in drag were determined by use of an integrating
manometer system that permitted pressures from either rake to be record-
ed photographically from the manometer. The drag data were, therefore,
obtained successively for the upper and lower rakes during a test run.
During the study of cyclic de-icing, data for each rake were obtained
with alternate cycles.

RESULTS

The data obtained in this study are presented in terms of the
increase in airfoil-section drag with duration in icing. The study is
divided into two primary categories: the first, which is concerned with
the drag increase for a swept airfoil (slat retracted), includes the
effect of ice formations on the unheated model as well as of the ice
formations associated with a cyclic de-icing system and a continuous-
heating system that does not evaporate all impinging water. The second
category, which is concerned with the drag increases of an airfoil with
an extended leading-edge slat, includes a brief description of the
effects of ice formations on the airfoil drag during a landing approach.
Wind-tunnel wall-interference effects on drag coefficients were not
evaluated.

General Considerations

As the geometric angle of attack of the airfoil was increased (slat
retracted),the effective angle of attack as indicated by droplet impinge-
ment patterns increased along the airfoil leading edge from the tunnel
floor to the tunnel ceiling. This phenomenon may be explained by the
fact that the sweep of the airfoil introduced a twist in the air stream
which was started by the farthest upstream portion of the model (near
floor) and became progressively greater as the air moved downstream and
encountered more of the airfoil.

The change in the effective angle of attack along the span caused
by the twist in the air stream was also evident from the section drag
coefficients for the bare airfoil calculated from the momentum wake
profiles (fig. 3). The lower rake behind the standard-airfoil section
(18 in. from tunnel floor) showed no appreciable drag change as the
geometric angle of attack was changed from 2° to 8°; whereas, the upper
rake behind the slatted-airfoil section, (24 in. from ceiling) indicated
a slightly larger drag than the lower rake at most of the low angles of
attack, a still larger drag coefficient at 7° angle of attack, and a
shift in momentum wake accompanied by a considerable increase in section

drag coefficient at 8°. The constant bare-airfoil drag coefficients obtained with the lower rake over the range of angle of attack shown in figure 3 are believed to have been caused by the twist in the air stream and possible interference effects of the tunnel floor on the air flow over the swept airfoil. These effects on drag coefficient have been observed with wake measurements for other swept airfoils (unpublished NACA data).

The icing characteristics of an unheated swept airfoil are different from those for an unswept airfoil. In reference 1, leading-edge glaze-ice formations on an unswept airfoil formed a continuous solid spanwise projection (fig. 4(a)); for a swept airfoil, a broken spanwise formation resembling a row of nested cups formed under similar conditions (fig. 4(b)). This phenomenon has been observed for other swept wings (fig. 4(c)), and apparently the spanwise distance between these cups increases as the sweep angle is increased. A similar broken, cup-shaped ice formation is shown on the airfoil with slat extended in figure 4(d). It is believed that as these rough glaze-ice deposits increase in size, local high spots are formed at intervals along the span because of a delay in the freezing of impinging water and a tendency to flow before solidification. These high points in the ice formation intercept more of the impinging water because of an increased local water-collection efficiency, and, as a result, adjacent ice deposits are shielded. The extent of shielding appears to be a function of the air-flow component parallel to the span as influenced by the sweep angle. A large sweep angle causes the shielding effect to extend farther along the span; hence, a greater separation is observed between the cups.

At low datum air temperatures (10° F) ice-formation characteristics of rime ice for a swept airfoil are the same as those observed for an unswept airfoil. At this low air temperature, the impinging droplets freeze upon striking the airfoil; consequently, the running wet condition associated with the collection of ice at air temperatures near the freezing point, required for the cup-shaped ice formation, does not occur.

Limitations of Thermal Icing-Protection System

The drag data reported herein were necessarily restricted by the limitations of the icing-protection system, especially with respect to the slatted portion of the model and for cyclic operation of the heating system. Inadequacies in the heating system are illustrated in figure 5 by the typical ice formations on insufficiently heated surfaces of the model. With the slat extended, the tracks were insufficiently heated even at a datum air temperature of 25° F and an airspeed of 175 miles per hour. The rear face of the slat (fig. 1(b)) was virtually unprotected by the cyclic de-icing system and accumulated sizable ice formations, partly by direct impingement in the slot and partly by runback

icing. These ice formations tended to decrease the slot exit area and, at times, prevented complete slat retraction by as much as 3 inches of travel. Similarly, the last 4 inches of the slat trailing edge on the upper surface accumulated runback icing that could not be dislodged except by large amounts of heat and long heating periods. The slat tabs were the worst offenders with respect to ice accumulation (fig. 5). These large ice masses could only be removed by exorbitant amounts of heating (unpublished data). During a cyclic de-icing test, these ice formations would shed sporadically after four to six cycles; however, the shedding would not occur simultaneously for all three tabs. The closing ribs at each end of the slat were insufficiently protected at datum air temperatures less than 20° F. The fixed airfoil section behind the slat was inadequately protected at the leading-edge region by the electric parting strips. A nonuniform distribution of heat to the lower surface of this portion of the model caused several cold areas that accumulated massive ice formations, especially near the track openings and at the airfoil skin over the track stations (fig. 5). At low datum air temperatures with slat extended, ice also formed on the insulated gas supply duct to the slat. The standard-airfoil (unslatted) portion of the model showed only two minor indications of inadequate heat distribution, namely, a rapid reduction in width of the gas-heated parting strip in the direction of gas flow and an inadequately heated strip of skin between the junction with the parting-strip fin and the entrance to the upper-surface double skin, which caused an ice ridge to remain after the rest of the airfoil was cleanly de-iced.

In conjunction with the limitations imposed by the heating system, a considerable inflow of air into the slot between the slat and the airfoil section behind the slat was observed, especially near the slat end adjacent to the standard-airfoil section. This three-dimensional flow characteristic caused the air to pass obliquely over the tracks and the slat hot-gas supply duct and thereby caused large wake effects, which were measured as part of the airfoil momentum wake loss by the upper rake. In an actual aircraft installation for which the tracks would be separated by 8 to 10 feet rather than the $1\frac{1}{2}$ feet for the model, these wake effects would be localized and would not constitute a large percentage of the over-all wake losses. Because of the wake effects caused by the tracks, the supply duct, and the large ice accretions on the inadequately protected areas of the model, a drag analysis with slat extended was rendered almost useless. The data presented for this mode of operation are merely indicative of the drag changes that are associated with the ice formations shown for each test run.

In addition to the heating-system deficiencies, difficulty was also experienced, during the latter part of the program, by hot-gas leaks through the valve supplying gas to the slat. The presence of these heat leaks caused large locally heated areas near the leading-edge region, which in some cases altered the resultant icing characteristics on the slat sufficiently to affect wake measurements.

Because of these model deficiencies, the present report may be
considered an extension of reference 1 to include a study of the drag
characteristics of a swept airfoil in icing conditions. Only limited
data are presented for the effect on drag of ice formations on the
extended slat.

Drag Measurements with Slat Retracted

Unheated airfoil, no parting strip. - The results of reference 1
indicate that the largest increases in section drag coefficient occur
in heavy glaze-icing conditions incurred at high datum air temperatures
(greater than 25° F) and high rates of water catch (liquid-water content
of the order of 0.8 g/cu m); consequently, the greatest effort expended
in the present study was to obtain additional drag information for these
glaze-ice conditions. The effects of glaze-ice formations on the section
drag of an airfoil are shown in figure 6 as a function of time in the
icing condition for a range of angle of attack from 2° to 8°. The data
were obtained for both airfoil sections with the slat fully retracted.
In general, the increase in drag is similar for both the slatted- and
standard-airfoil sections for a range of angle of attack from 2° to 6°.
The initial rate of change of the drag coefficient in icing for both
airfoil sections at 8° angle of attack is somewhat similar; however, the
drag for the standard-airfoil section is almost linear with respect to
time in icing, whereas the drag for the slatted-airfoil section does not
change appreciably after the initial 2 to 3 minutes in the icing condi-
tion. The rate of change of the section drag coefficient increases with
an increase in angle of attack from an average drag change of 0.015 for
10 minutes in icing at an angle of attack of 2° to 0.025 at 8° (standard
airfoil). These drag changes represent 167- and 278-percent increases
in section drag coefficient, respectively, for 10-minute icing periods
with a liquid-water content of 0.83 gram per cubic meter at a datum air
temperature of 25° F. Photographs of the ice formations associated with
the drag coefficients of figure 6 are presented in figure 7 for angles
of attack of 2°, 4°, 6°, and 8°. (The standard-airfoil section is seen
in the lower portion and the slatted-airfoil section in the upper por-
tion of each set of photographs.) The glaze-ice formations generally
protrude into the flow field and cause disruptions to the air flow, which
result in large drag increases. In reference 1, a shift in the position
of the momentum wake (indicative of a loss in lift) is reported to
accompany large increases in drag at an angle of attack of 8° for a
heavy glaze-icing condition on an unswept airfoil; this shift was not
evident for the standard-airfoil section (lower rake station). The
slatted-airfoil section (upper rake station), however, showed a large
increase in drag and the onset of stall at an angle of attack of 8°,
even in dry air.

The effect of a rime-ice formation on airfoil drag is also shown in figure 6 by the change in section drag coefficient obtained at an angle of attack of 4° with a datum air temperature of 10° F and a liquid-water content of 0.55 gram per cubic meter. The average increase in drag coefficient in the rime-icing condition was 0.0068 (61 percent) in 10 minutes of icing. Photographs of the rime-ice formations associated with the rime-ice drag data presented in figure 6 are shown in figure 8. The primary rime-ice formations blend smoothly into the airfoil contour and do not protrude into the flow field in the manner of the heavy glaze-ice formations previously discussed.

The section drag measurements indicated that, even at relatively low rates of water catch (0.39 g/cu m, fig. 9), appreciable increases in section drag coefficient occurred during icing periods up to 20 minutes in duration. The section drag coefficient increased an average of about 15 percent in the initial 3 minutes of the icing period. The largest increase in section drag coefficient occurred at an angle of attack of 4° after 14 minutes in the icing condition, amounting to a 76-percent increase. A sequence of photographs showing the progressive build-up of the ice formations associated with the drag values of figure 9 are shown in figure 10 for angles of attack of 4° and 8°. The photographs indicate that the glaze-ice formations formed at a water content of approximately 0.39 gram per cubic meter are faired somewhat into the general airfoil contour in the stagnation region.

Unheated airfoil with parting strip. - Studies were made to determine whether the leading-edge-region ice formations obtained during use of an ice-free parting strip such as recommended for cyclic de-icing systems (refs. 2 to 4) were more or less detrimental than those obtained without a parting strip. The results of a study with an ice-free parting strip are shown in figure 11, wherein the section drag coefficient is shown as a function of time in icing for angles of attack of 4° and 8°. The data presented were obtained at a datum air temperature of 25° F and at two liquid-water contents (approx. 0.4 and 0.85 g/cu m) for both slatted- and standard-airfoil sections. The average rate of change of the drag coefficient with time is approximately the same as with a completely unheated airfoil (fig. 6). Only at an angle of attack of 8° with a high rate of water catch and after $7\frac{1}{2}$ minutes in icing (fig. 11(a)) does the drag increase more rapidly with a parting strip than without; however, this increased rate may be only an exceptional case. From these data and the similar results of reference 1, it may be concluded that the ice formations associated with an ice-free parting strip are no more detrimental than those formations obtained with an unheated leading-edge section. Photographs showing the ice-free parting strip and the resultant stagnation-region ice formation associated with the drag data of figure 11 are presented in figure 12. As the ice builds up on either side of the narrow parting strip (1 in.), the ice-free area is gradually

reduced in size. During the latter part of most of these runs, the parting strips were obliterated because of ice-bridging between the upper and lower surfaces.

Cyclic de-icing. - For a cyclically de-iced leading-edge section utilizing an ice-free parting strip and with the slat retracted, the increases in section drag coefficients caused by primary and runback ice formations are shown in figure 13 as a function of icing time. Photographs of the ice formations corresponding to the drag data in figure 13 are shown in figure 14. Because the wake survey data for the cyclic de-icing runs were recorded for the first cycle with one rake (before and after the heat-on period) and for the following cycle with the other rake, the drag-coefficient curves for each airfoil section are discontinuous, with only every other cycle recorded.

For glaze-ice formations occurring at a datum air temperature of 25° F, a liquid-water content of 0.39 gram per cubic meter, and an angle of attack of 4°, the section drag coefficient at the end of the heat-on period increased less than 6 percent after a 20-minute icing time (fig. 13(a)). Removal of the ice formation by intermittent heating showed an insignificant effect on the drag values. An increase in the heat-off period from 220 to 460 seconds caused an increase in drag of as much as 0.0047 at the end of the heat-off period (fig. 13(a)). The ice formations contributing this drag increase are shown in figure 14(a). Shedding of these ice formations caused the drag to return to within 11 percent of the airfoil-section drag in dry air. A decrease in the heating period from 20 to 10 seconds did not materially change the drag value after shedding of the ice from that obtained at the longer heat-on period (fig. 13(a)). The ice formations associated with the drag values incurred during the heat-off period of 470 seconds are shown in figure 14(a).

The effect on the drag coefficient of an increase in liquid-water content from 0.39 to 0.80 is shown in figure 13(b) for the airfoil at an angle of attack of 4°. With a 20-second heat-on period, the maximum increase in drag coefficient for the standard-airfoil section was only 3 percent after ice removal for an icing exposure time of $12\frac{1}{2}$ minutes. The maximum drag increase during the heat-off period amounted to 0.0024. A decrease in heating period from 20 to 10 seconds did not materially affect the airfoil drag (fig. 13(b)). The drag values for the slatted-leading-edge section with slat retracted (upper rake) showed a much greater drag increase during the heat-off period for a liquid-water content of 0.80 (maximum increase of 0.013) than for 0.39 gram per cubic meter. This increase is believed to be caused by the shape of the ice formation on the upper surface (fig. 14(b)). The drag after ice removal also increased with time, reaching a value after $36\frac{1}{2}$ minutes in the icing condition of 0.0044 higher than the airfoil drag value in dry air.

Observations showed that the ice formation in the slatted-leading-edge region is distorted because of the warm areas caused by the leaking gas valve. This distortion of the ice formations caused the ice to protrude more perpendicularly into the flow field around the airfoil leading-edge region and thereby disrupt the flow and cause large drag increases.

At an angle of attack of 2^O with slat retracted and a liquid-water content of approximately 0.80 gram per cubic meter (fig. 13(c)), the slatted-airfoil drag increase following the heating period (20 sec) was approximately the same as at the 4° angle of attack. The ice formations in the leading-edge region for an angle of attack of 2^O are shown in figure 14(c); they are similar to those at 4°, except that the primary ice formations are shifted around the leading edge in a direction toward the upper surface. Incomplete ice shedding on the standard-airfoil section accounted for the higher drag values following successive heating periods.

Continuous heating. - The drag increase attributable to runback ice formations was determined for the standard-airfoil section for a continuous-heating system that does not evaporate all the impinging water. The study was made for a liquid-water content of 0.80 gram per cubic meter and angles of attack of 4° and 7°. In addition, one run was made at 6° angle of attack with a liquid-water content of 1.05 grams per cubic meter. Such runback icing may be encountered in flight when an anti-icing system is thermally submarginal for the icing condition. The heat input to the airfoil was progressively reduced, and the drag-increase measurements were coordinated with photographs of the ice formations. The drag data are plotted in figure 15 as a function of time in icing; the accompanying photographs for the runs at 4° and 7° angles of attack are shown in figure 16.

At a 4° angle of attack and with a heating rate of 10,300 Btu per hour per foot span for the standard airfoil and a combined heating rate of 11,380 Btu per hour per foot span for the slat and airfoil section behind the slat, no significant changes in drag were observed during 10 minutes in icing (fig. 15(a)). A small drag increase for the standard-airfoil section (maximum of 15-percent increase in $17\frac{1}{2}$ min of icing) occurred with the heat input reduced to 7670 Btu per hour per foot span (74 percent of initial value). For the slatted section of the airfoil, the drag increased markedly when the combined heat input was reduced to 6660 Btu per hour per foot span (59 percent), the drag increase amounting to 0.0067 (73 percent) in the same $17\frac{1}{2}$-minute icing period. A further 20 minutes with this reduced heat input caused the slatted-section drag to increase an additional 0.0028. During the same 20-minute icing period, the standard-airfoil heating rate was reduced to about 46 percent of the initial value, with a consequent increase in drag from 0.0093 to 0.0148 (59 percent). It is apparent from the data of figure 15(a) and the lower photographs of the ice formations in figure 16(a) that the large increases in drag were caused primarily by the lower-surface ice formations.

An increase in the heating rate caused a reduction in drag (fig. 15(a)) by removing much of the ice on the lower surface. The section drag coefficient of the standard airfoil did not change appreciably at a 6° angle of attack until a heat-input value of 5170 Btu per hour per foot span was reached (32 percent of initial heating rate, fig. 15(b)). A further reduction in heat input to 2850 Btu per hour per foot span caused the drag coefficient to increase from about 0.0130 to 0.0177 in an additional 10 minutes.

At an angle of attack of 7° (fig. 15(c)) with a heating rate varied downward from 17,500 to 7550 Btu per hour per foot span, no appreciable drag changes were observed for the standard-airfoil section. For the slatted section, however, the drag increased with time in icing even with a heating rate of 18,840 Btu per hour per foot span (combined heating rate for slat and airfoil section behind slat). This increase in drag was caused by the near stall condition of the airfoil at this angle of attack; hence, small amounts of runback icing on the upper surface easily induced flow separation, with a consequent rapid increase in drag. As the heating rate continued to be reduced, the drag of the slatted section reached a value of 0.039 (combined heating rate of 4290 Btu/(hr) (ft span)) or 172-percent increase over the initial section drag coefficient. As the heating rate of the standard airfoil was also progressively reduced to 5380 and 2920 Btu per hour per foot span, the drag coefficient increased progressively, as shown in figure 15(c), a maximum section drag coefficient of 0.0201 (95-percent increase) being reached at the end of the $54\frac{1}{2}$-minute icing time. Photographs of the ice formations causing these drag values are shown in figure 16(b). A correlation of the data of figure 15 with the photographs of figure 16(b) indicates that the initial drag increases for the standard-airfoil section were, caused primarily by ice formations on the lower surface in conjunction with light runback icing on the upper surface. The final large drag increase was caused by heavy ice formations on both surfaces.

Drag Measurements with Slat Extended

Unheated airfoil. - The study of the effect of ice formations on the drag coefficient of the slatted leading-edge section of the model was generally limited to an angle of attack of 6° and a partial extension of the slat (halfway, 8°). The initial drag (dry air) shows that extension of the slat (fig. 17) caused a threefold increase in drag over the value with slat retracted (fig. 3). Most of this increase in drag was caused by the previously discussed wake effects attributed to the air flow over the tracks and the hot-gas supply duct to the slat. The drag increases with time in icing for the unheated slat with and without an ice-free parting strip are shown in figure 17 for a datum air temperature of 25° F and a liquid-water content of 1.05 grams per cubic meter. The slat

tracks were heated to minimize the local ice formations on the tracks.
The data again indicate little difference between the average values of
the rate of change in drag coefficient for operation with or without a
parting strip.

Comparison of the data of figures 6 and 17 indicates that the rate
of change in drag with time appears to be slightly greater with the slat
extended than with the slat retracted. In general, however, these
values are similar enough to warrant the belief that, for the conditions
studied, the extension of the slat has no great effect on rate of drag
increase caused by icing. A lower rate of water catch (water content
reduced from 1.05 to 0.45 g/cu m) resulted in a section-drag-coefficient
increase of only about 0.0045 above the initial value for 21 minutes
in icing. Photographs of the ice formations incurred during the drag
study shown in figure 17 are presented in figure 18. The effect of hot-
gas leaks into the slat is evidenced by the large ice-free areas in the
leading-edge region.

Cyclic de-icing. - The effects on drag of primary and residual
runback-ice formations with the slat extended halfway (8°) and with the
airfoil at an angle of attack of 6° are shown in figure 19 as a function
of icing time for liquid-water contents of 1.05, 1.23, and 0.64 grams
per cubic meter. Photographs of the ice formations before and after
heating periods corresponding to some of the drag values of figure 19(a)
are shown in figures 20(a) and (b). The ice-free parting strip for
these studies was generally too wide because of the heat leaks into the
slat. No significant differences in drag were observed for the rela-
tively small change in water content. The high drag values for the
slatted part of the model after ice removal were caused by the residual
ice formations on the lower surface of the slat, on the slat tabs, and
around the track openings (lower right fig. 20(a) and upper right fig.
20(b)). Removal of ice on the upper surface was incomplete, as evi-
denced by runback streaks of ice 6 to 8 inches long starting about 4
inches aft of the leading edge, and also on the last 4 inches of the
slat trailing edge. The large drag values following ice removal were
caused by heavy residual ice formations on the slat tabs.

The effect on drag of an increase in the heating period from 12
seconds (fig. 19(a)) to 18 seconds is shown in figure 19(b). Photographs
of the ice formations associated with the longer heating period before
and after ice removal are shown in figure 20(c). A comparison of fig-
ures 20(a) and (c) shows that much less residual ice remains on both
surfaces of the slat with a heating period of 18 seconds than with 12
seconds. The slat drag data, however, do not indicate any decrease in
drag except for the first cycle.

With a reduction in datum air temperature from 25° to 10° F and
a liquid-water content of 0.64 gram per cubic meter, the drag values for

the slatted leading-edge section increased with icing time as shown in
figure 19(c). Cyclic removal of the ice did not appreciably decrease
the drag because of the ice on the lower surface of the slat, on the
tabs, around the track openings,and on the tracks. These ice formations
are shown in figure 20(d) both before and after the heating period.

Continuous heating. - At an angle of attack of 6°, slat extension
halfway, and a heating rate of 14,640 Btu per hour per foot span (com-
bined heat input to slat and airfoil section behind slat) the drag coef-
ficient for the slatted section of the model increased rapidly with time
in an icing condition of 1.05 grams per cubic meter, as shown in fig-
ure 21. After $16\frac{1}{4}$ minutes in the icing condition, the drag had increased
from 0.030 to 0.039. This increase in drag was caused by ice formations
on the slat tabs and small ice accretions on the rearmost $1\frac{1}{2}$ inches of
the slat upper surface. Reductions in heat input to 9780, 6840, and
4960 Btu per hour per foot span caused a continued increase in drag
(fig. 21) and increased the extent of the runback on the slat upper sur-
face. The ice formations causing these increases in drag are shown in
figure 22.

Let-Down - Approach Condition

With the slat retracted, studies were made of simulated let-down -
approach conditions for glaze-icing conditions, during which the unheated
airfoil was allowed to ice for varying periods at low angles of attack
(2^O and 4°) and then the attitude was increased to 7° or 8°. At low
liquid-water contents (low rates of water catch) the resultant drag
values at the increased angle of attack were on the same order of mag-
nitude as those normally obtained by initially starting at the high
angle of attack. Cyclic removal of the ice formations returned the
drag values to those normally associated with the residual runback ice
formations at the high angle of attack. For glaze-ice formations at
high rates of water catch, the drag value for the slatted-airfoil sec-
tion at 2^O angle of attack and an airspeed of 260 miles per hour after
4 minutes of icing amounted to about 0.0135 and increased to 0.062 when
the angle of attack was increased to 8° and the speed decreased to 175
miles per hour. The slat was then extended halfway (still with the ice
formation incurred at 2^O), with a slight decrease in drag coefficient to
0.057. Full slat extension (16°) increased the drag coefficient to
0.090. The drag coefficient for the standard airfoil was not greatly
affected by a change in attitude. Similar results were obtained when
the initial ice formations were incurred at an angle of attack of 4°.

DISCUSSION

In general, the section drag characteristics of the swept NACA 63A-009 airfoil with slat retracted are more adversely affected by the presence of ice formations in the leading-edge region than are those of the unswept NACA 65_1-212 airfoil (ref. 1). At low rates of water catch, the rate of drag increase for the unheated swept 63A-009 airfoil is approximately $2\frac{1}{2}$ times as great as that of the unswept airfoil of reference 1 for similar icing conditions. Several factors are believed to contribute to the greater rate of drag change for the 63A-009 airfoil. The chord of the swept 63A-009 airfoil was approximately 14 percent smaller and the thickness was 25 percent less than those of the unswept 65_1-212 airfoil. The effect of these reductions in size is to yield a higher drag value for a constant ice or protuberance size (see refs. 1 and 6 for the effect of protuberance height on drag values). In addition, the three-dimensional effects introduced by airfoil sweep probably result in an increase in the length of the boundary-layer path over the leading-edge-region over that occurring with two-dimensional flow; hence, the disruptive effects on the boundary layer by the ice formations in the leading-edge region are probably greater and contribute to the greater drag values.

The results reported herein corroborate the data of reference 1, which show that a heavy glaze-ice formation resulting from icing encounters with combinations of high liquid-water content, large droplet size, high airspeed, and high datum air temperatures will cause large and rapid increases in drag that may be detrimental to aircraft operation. Also, the operation of an aircraft with glaze ice on the leading-edge region in a landing-approach condition should be avoided in order to minimize the possibility of airfoil stall due to these ice formations.

In order to compare a continuous-heating system with a thermal cyclic de-icing system in an operational analysis, the relation between the rate of change of drag with the heating rate is required. From the continuous-heating data of figures 6 and 15, the average time rate of change in drag coefficient can be determined as a function of heating rate, as shown in figure 23. These data are for moderate to high rates of water catch and include angles of attack of 4°, 6°, and 7°. Within a reasonable scatter, the data for the standard-airfoil section appear to fall on a single curve over most of the range shown. No apparent drag increase is indicated for a heating rate greater than 9000 Btu per hour per foot span; whereas, with no heating, the data indicate some variation in drag increase per unit time with angle of attack (fig. 6). Although the residual ice formations for heating rates of about 3000 Btu per hour per foot span are relatively large (see fig. 16(b)), the rate of drag increase is only of the order of 30 percent of the drag increase for an unheated airfoil. The limit of heating rate for zero

drag increase (around 9000 Btu/(hr)(ft span)) is somewhat doubtful, since the afterbody of the airfoil was heated to prevent frost accumulations; consequently, runback ice formations beyond the gas-heated leading-edge section (20 percent of chord) could not be evaluated. Only a single reliable data point (fig. 23) at a 4° angle of attack was obtainable for the slatted-airfoil section with the slat retracted and with continuous heating. It is believed that data for the slatted-airfoil section lie somewhat higher than those for the standard-airfoil section because of the peculiarities in the air flow over the swept model. It also appears probable that additional data may indicate separate curves for each angle of attack, especially at low heating rates (less than 5000 Btu/(hr)(ft span)).

With figure 23 it is possible to compare heating rates for continuous-heating systems with those for cyclic de-icing systems on the basis of drag increase. Drag increase with time typical of a cyclic de-icing system (taken from fig. 13(b)) is shown by the dotted lines in figure 24 for both airfoil sections. The average drag coefficient for cyclic de-icing is shown by the solid lines. The instantaneous heating rate for cyclic de-icing was about 25,400 Btu per hour per foot span for the slatted-airfoil section and 24,100 Btu per hour per foot span for the standard-airfoil section; however, in terms of equivalent continuous-heating rates (based on cycle ratio, ref. 3), these rates become 2120 and 2010 Btu per hour per foot span, respectively. Based on data from figure 23, the average drag coefficient for a continuous-heating system can be shown by straight lines (fig. 24) originating with the bare airfoil drag coefficient and depending on the heating rate for their slope. Curves of the average drag increase for two continuous-heating rates, 3500 and 5000 Btu per hour per foot span, are shown in figure 24 for both airfoil sections. For the slatted-airfoil section, points of equal drag penalty during the icing encounter, shown by the intersections of the drag-penalty curves for the continuous-heating system with the curve of the cyclic de-icing system, occur at 8.7 and 12 minutes, respectively, for the two heating rates given previously. For the standard-airfoil section, the point of equal drag penalty occurs at about 4.7 minutes with the higher heating rate; whereas, at the lower heating rate, the average drag increase with continuous heating is always greater than the average drag increase with cyclic de-icing.

For the standard-airfoil section with a heating rate of 5000 Btu per hour per foot span, since the drag increase for both systems is substantially the same for the first 4 minutes of the icing encounter, the heat savings obtained with the cyclic de-icing system over the continuous-heating system can be shown by a direct comparison of the heating rate (2120 to 5000 Btu/(hr)(ft span), respectively) and is in the ratio of 1:2.36. Similar trends and observations are shown for the slatted-airfoil section in figure 24(a). The drag penalty due to residual ice formations following emergence from the icing encounter is even more

evident than for the standard-airfoil section. The drag increase due to residual ice formations for the cyclic de-icing system is approximately 0.0012 after $16\frac{1}{2}$ minutes in icing; whereas, with the continuous-heating system at a heating rate of 3500 Btu per hour per foot span, the drag increase due to residual icing is 0.0104 and with 5000 Btu per hour per foot span is 0.0076.

From comparisons such as this, it is possible to evaluate the heat savings that may be expected from a cyclic de-icing system. For operation in icing conditions exceeding the time at which the average drag coefficients are equal for the two systems, the continuous-heating system that does not evaporate all impinging water will always suffer a performance penalty that will become increasingly more severe with time in icing. It should be noted that comparisons such as these apply during the icing encounter; and, after emergence from the encounter and cyclic removal of the ice formations, only a slight drag penalty due to residual ice formations may exist; whereas, the drag penalty for the continuous-heating system remains until the long process of sublimation has removed the residual ice formation.

It must be emphasized also that the values cited in these examples are for the specific model and conditions described herein and have limited application to other airfoils and conditions. Although the method of comparison shown in figure 24 should be valid, there is need for additional data to permit thorough evaluation of continuous-heating and cyclic de-icing systems for operational analyses.

SUMMARY OF RESULTS

The results of a study of the effects of ice formations on the section drag of a 36° swept NACA 63A-009 airfoil with partial-span leading-edge slat may be summarized as follows:

1. Glaze-ice formations in the leading-edge region of the airfoil caused large and rapid increases in section drag coefficient. In general, the icing of thin swept airfoils will result in greater aerodynamic penalties than for thick unswept airfoils. The change in drag coefficient in icing conditions for the swept 63A-009 airfoil with slat retracted was of the order of $2\frac{1}{2}$ times as great as that for an unswept 65_1-212 airfoil.

2. Removal of the primary ice formations by cyclic de-icing caused the drag to return almost to the bare-airfoil drag coefficient. The increment of drag increase remaining after the heating period was caused by residual runback ice formations and ice remaining on the surface because of limitations of the heating system.

3. The section drag coefficient for the unheated airfoil in icing conditions was substantially unaffected by the use of an ice-free parting strip at the stagnation region.

4. With the slat extended, initial (dry air) drag coefficient values were increased threefold over the drag values with slat retracted because of wake effects caused by the slat tracks and the hot-gas supply line; consequently, an evaluation of absolute drag of the slatted-airfoil section was impossible. The rate of change in drag coefficient in icing conditions with the slat extended was of the same order of magnitude as with the slat retracted.

5. A glaze-ice formation on the leading-edge section for a let-down and approach condition, during which the airfoil angle of attack is increased from low to high angles of attack (7° or 8°), caused a large increase in section drag coefficient, especially when the slat was extended at the high angle of attack.

Lewis Flight Propulsion Laboratory
    National Advisory Committee for Aeronautics
        Cleveland, Ohio, November 4, 1953

REFERENCES

1. Gray, Vernon H., and von Glahn, Uwe H.: Effect of Ice and Frost Formations on Drag of NACA 65_1-212 Airfoil for Various Modes of Thermal Ice Protection. NACA TN 2962, 1953.

2. Gray, V. H., Bowden, D. T., and von Glahn, U.: Preliminary Results of Cyclical De-Icing of a Gas-Heated Airfoil. NACA RM E51J29, 1952.

3. Gray, Vernon H., and Bowden, Dean T.: Comparison of Several Methods of Cyclic De-Icing of a Gas-Heated Airfoil. NACA RM E53C27, 1953.

4. Lewis, James P., and Bowden, Dean T.: Preliminary Investigation of Cyclic De-Icing of an Airfoil Using an External Electric Heater. NACA RM E51J30, 1952.

5. Block, Myron J., and Katzoff, S.: Tables and Charts for the Evaluation of Profile Drag from Wake Surveys at High Subsonic Speeds. NACA WR L-107, 1945. (Supersedes NACA RB L5F15a.)

6. Jacobs, Eastman N.: Airfoil Section Characteristics as Affected by Protuberances. NACA Rep. 446, 1932.
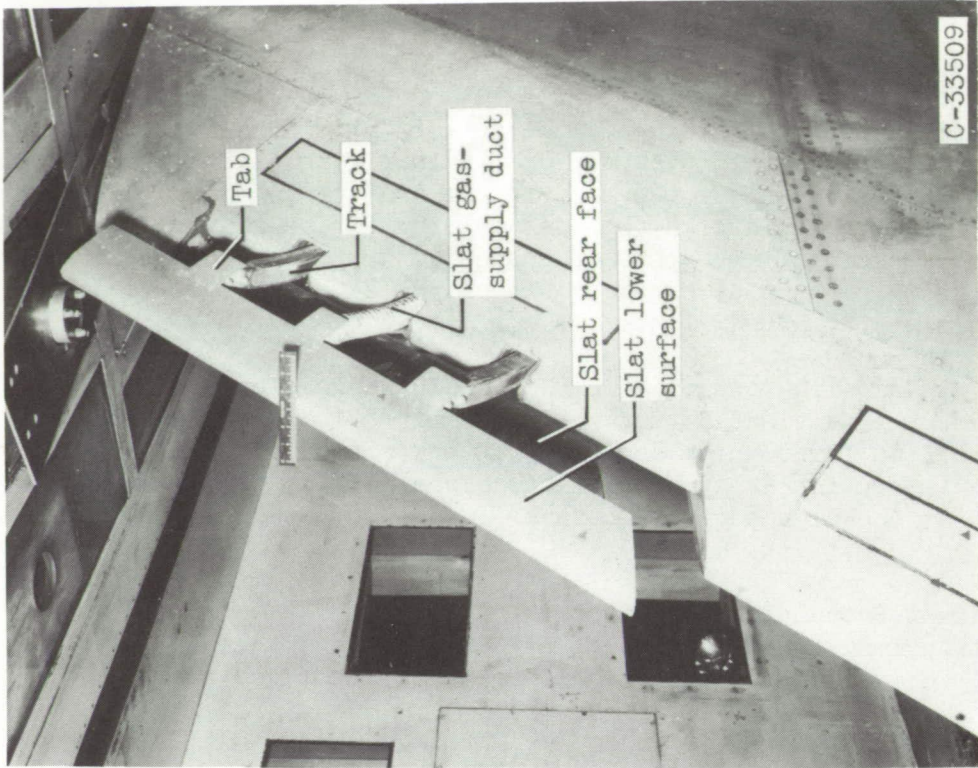
(b) Lower surface.

(a) Upper surface.

Figure 1. - Installation of swept airfoil with partial-span leading-edge slat in icing tunnel.
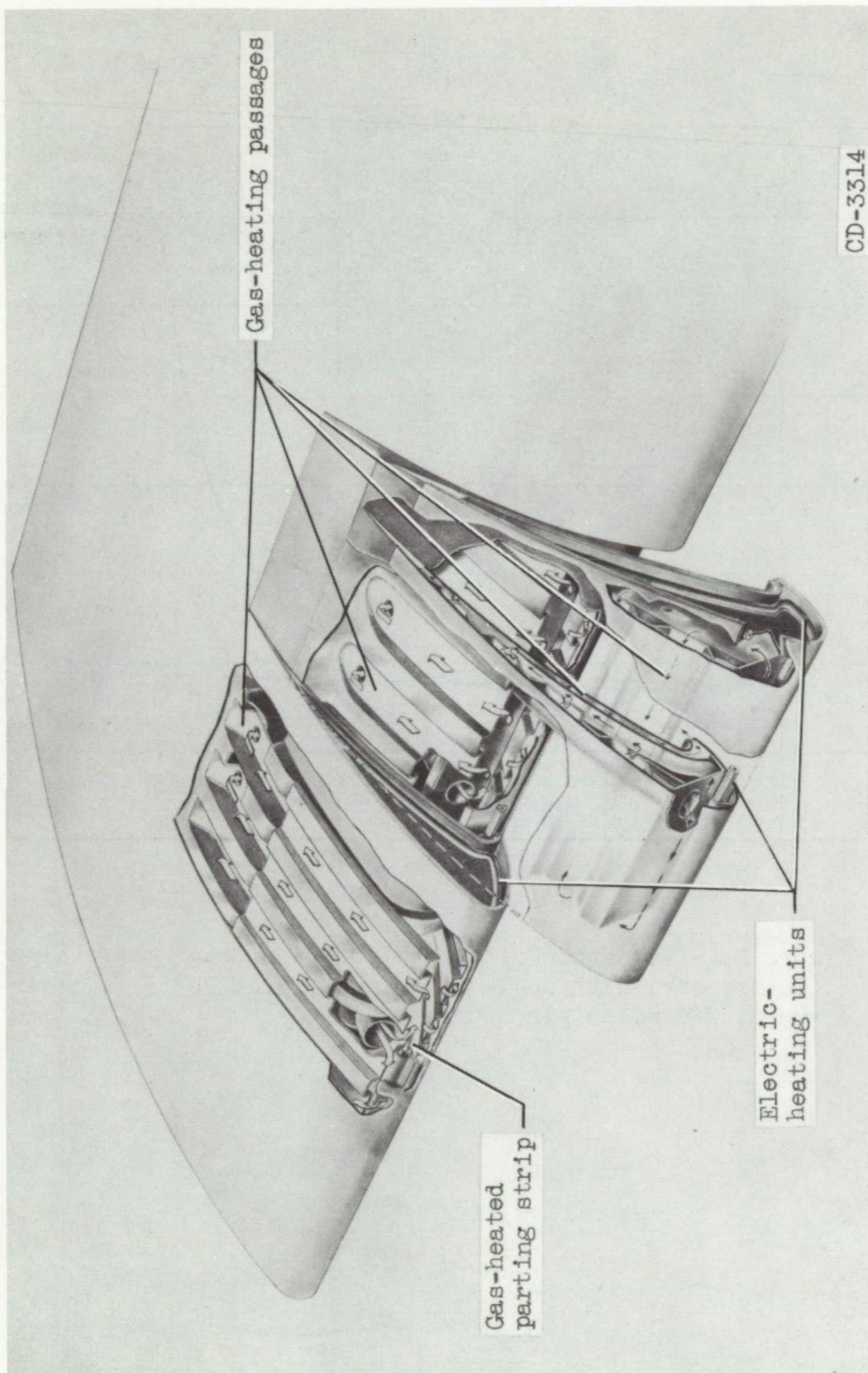
Figure 2. - Cutaway drawing of model showing heating passages.
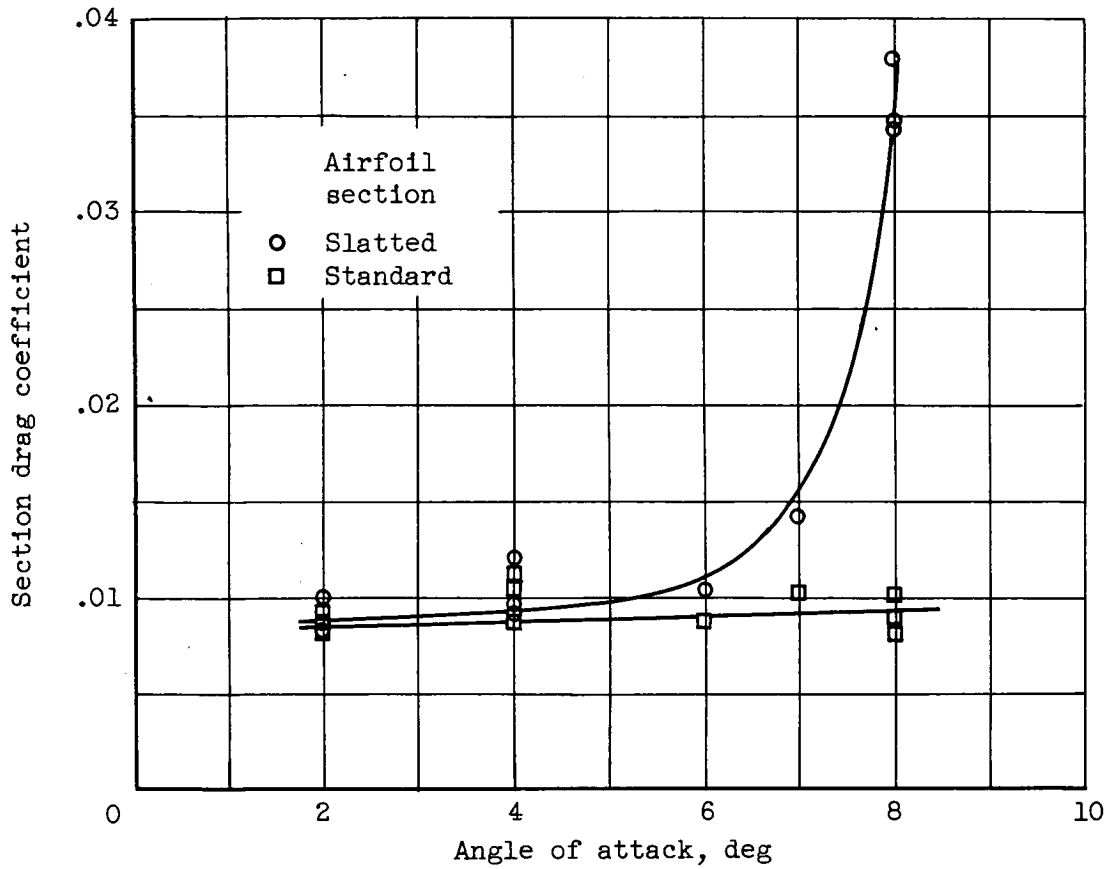
Figure 3. - Variation of airfoil-section drag coefficient
(in dry air) with angle of attack. Slat retracted; air-
speed, 260 miles per hour.
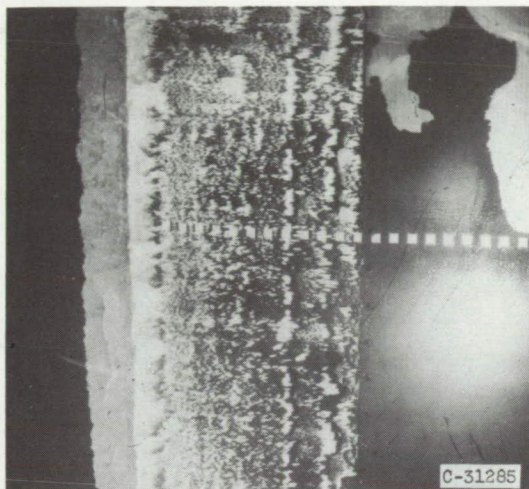
(a) Sweep angle, 0°.

(b) Sweep angle, 36°.
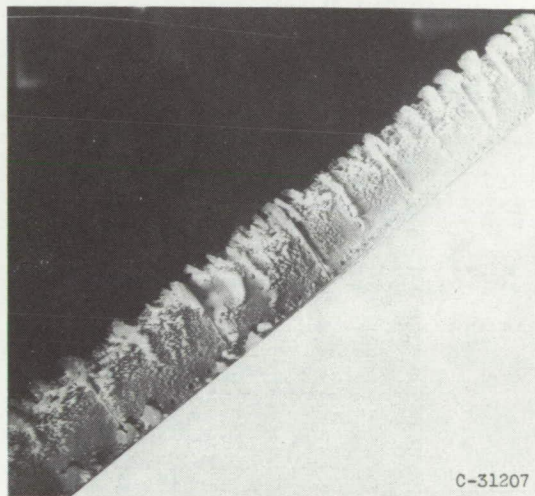
(c) Sweep angle, 60°.

Figure 4. - Typical heavy glaze-ice formations on various unheated airfoil leading-edge and lower surfaces, illustrating effect of airfoil sweep angle on physical characteristics of ice formation.

(d) Close-up of ice formations on slatted leading edge with 36° sweep.

Figure 4. - Concluded. Typical heavy glaze-ice formations on various
unheated airfoil leading-edge and lower surfaces, illustrating effect
of airfoil sweep angle on physical characteristics of ice formation.
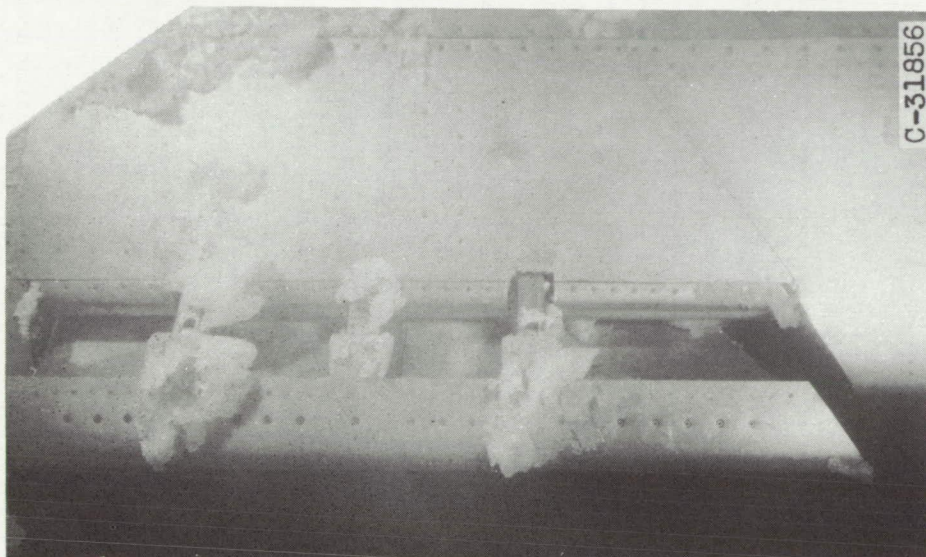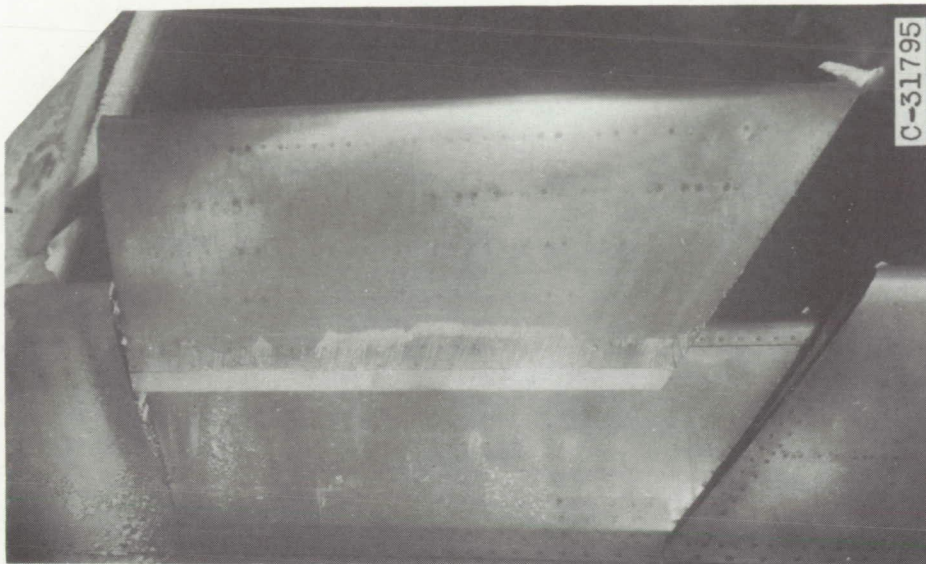
(b) Upper surface.

(a) Lower surface.

Figure 5. - Location and magnitude of ice formations on insufficiently heated areas of airfoil surfaces.
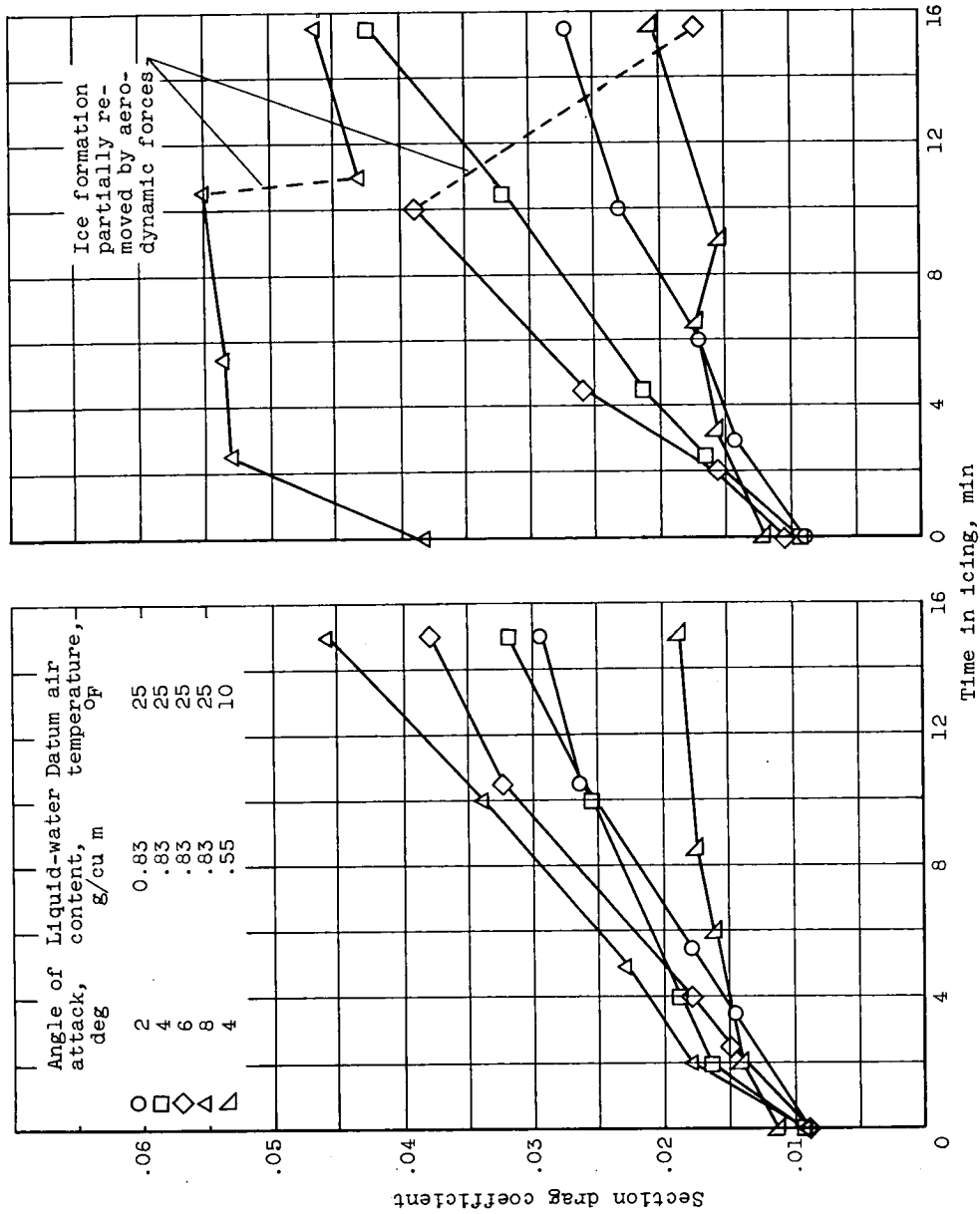
(a) Standard-airfoil section.   (b) Slatted-airfoil section.

Figure 6. - Variation of section drag coefficient with time in icing for unheated airfoil (slat retracted) at a high rate of water catch. Airspeed, 260 miles per hour.
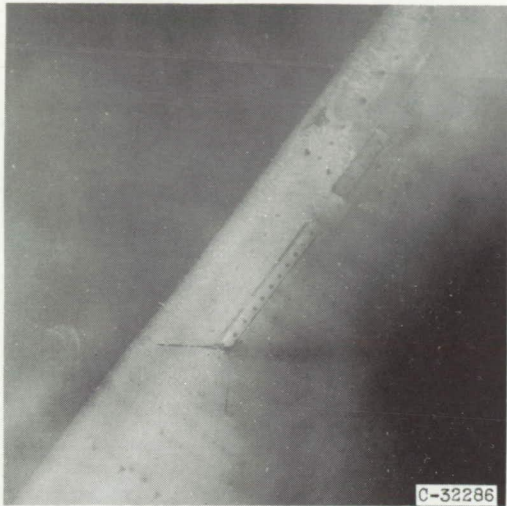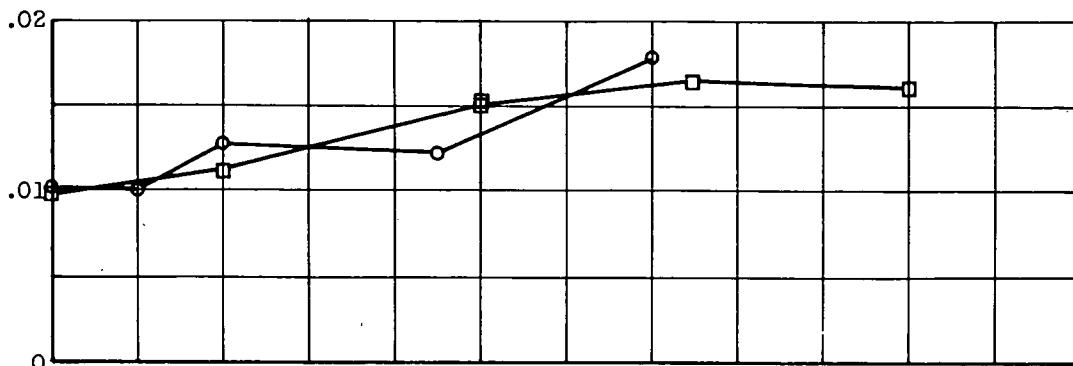
Lower surface. Icing time, $3\frac{1}{2}$ minutes;
section drag coefficient, 0.0145.
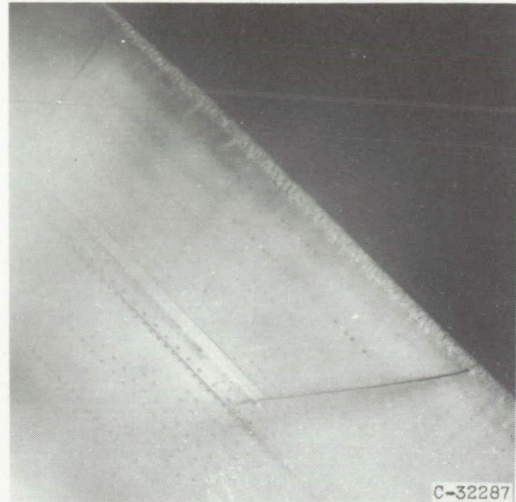
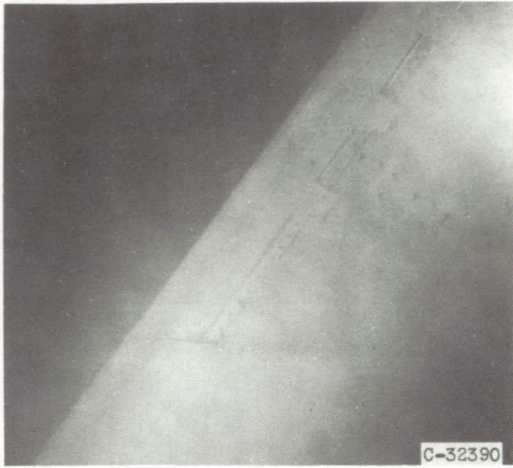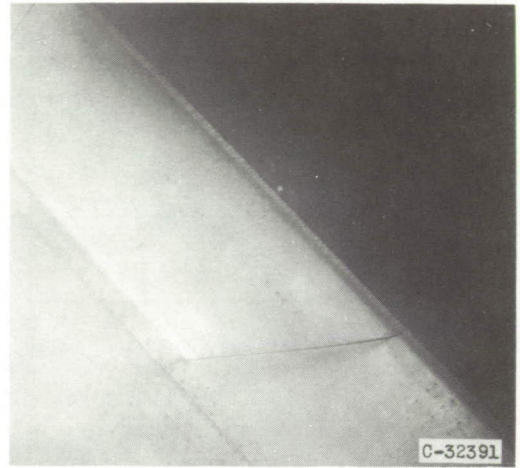Upper surface. Icing time, $5\frac{1}{2}$ minutes;
section drag coefficient, 0.0177.
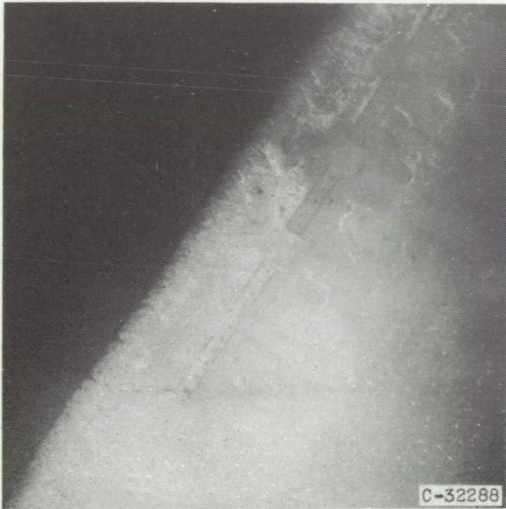
Lower surface. Icing time, 10 minutes;
section drag coefficient, 0.0251.
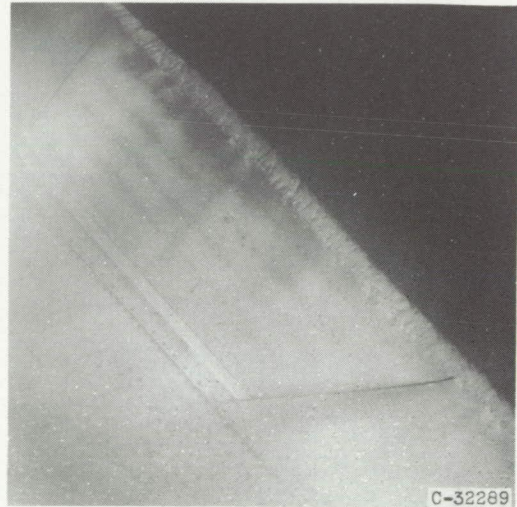
Upper surface. Icing time, $10\frac{1}{2}$ minutes;
section drag coefficient, 0.0265.

(a) Angle of attack, 2°; initial standard-airfoil-section drag
coefficient, 0.0090.

Figure 7. - Typical glaze-ice formations with high rate of water catch on
unheated airfoil leading-edge section (slat retracted). Airspeed, 260
miles per hour; datum air temperature, 25° F; liquid-water content,
0.83 gram per cubic meter.
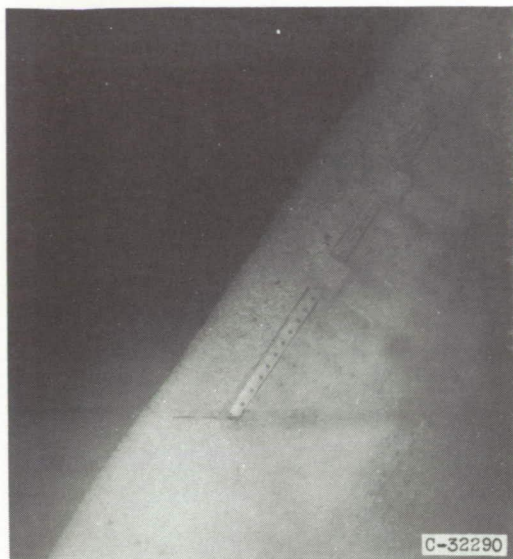
Lower surface. Icing time, $4\frac{1}{2}$ minutes;
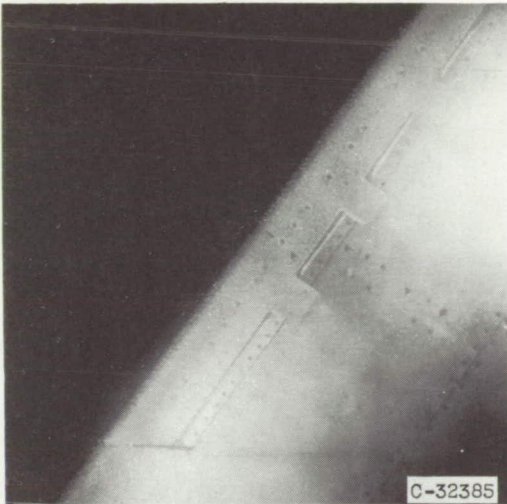section drag coefficient, 0.0192.
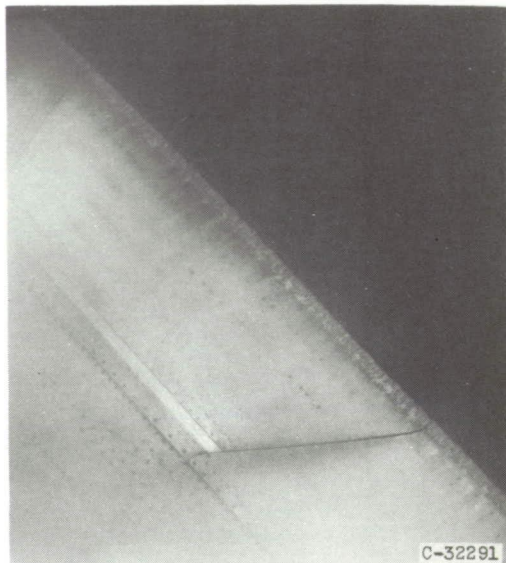
Upper surface. Icing time, 5 minutes;
section drag coefficient, 0.0199.
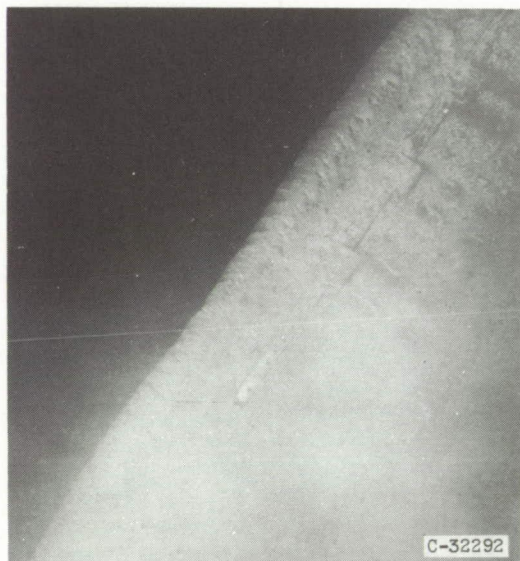
Lower surface. Icing time, 10 minutes;
section drag coefficient, 0.0252.
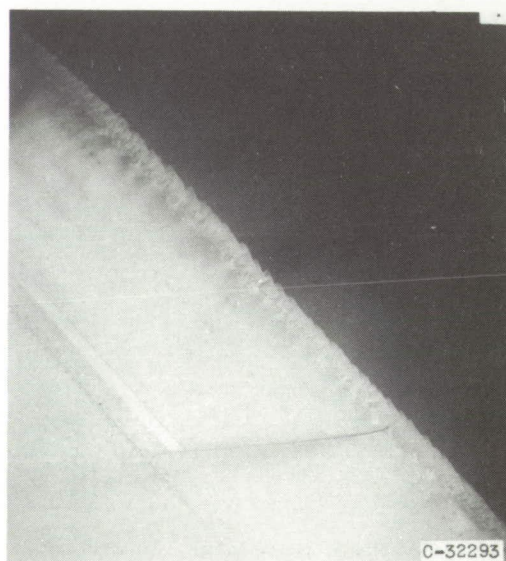
Upper surface. Icing time, $10\frac{1}{2}$ minutes;
section drag coefficient, 0.0260.

(b) Angle of attack, 4°; initial standard-airfoil-section drag
        coefficient, 0.0091.

Figure 7. - Continued. Typical glaze-ice formations with high rate of
     water catch on unheated airfoil leading-edge section (slat retracted).
     Airspeed, 260 miles per hour; datum air temperature, 25° F; liquid-
     water content, 0.83 gram per cubic meter.
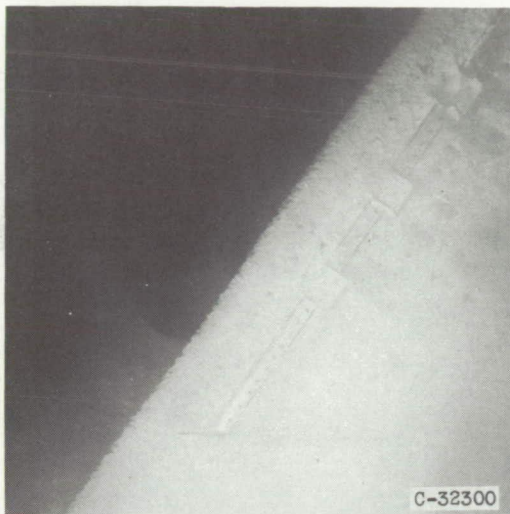
Lower surface. Icing time, 4 minutes;
section drag coefficient, 0.0177.

Upper surface. Icing time, $4\frac{1}{2}$ minutes;
section drag coefficient, 0.0188.
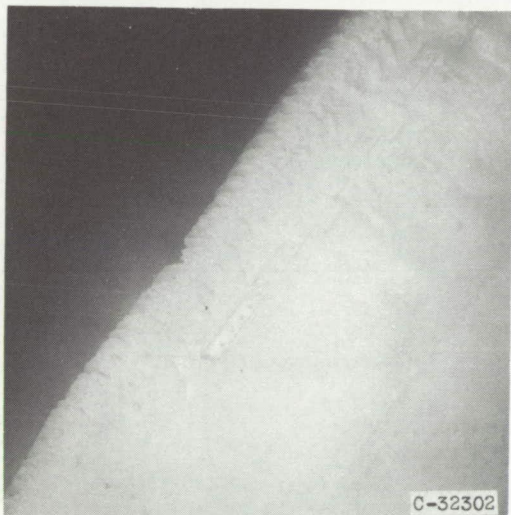
Lower surface. Icing time, 10 minutes;
section drag coefficient, 0.0311.

Upper surface. Icing time, $10\frac{1}{2}$ minutes;
section drag coefficient, 0.0321.

(c) Angle of attack, 6°; initial standard-airfoil-section drag
   coefficient, 0.0089.

Figure 7. - Continued. Typical glaze-ice formations with high rate of
   water catch on unheated airfoil leading-edge section (slat retracted).
   Airspeed, 260 miles per hour; datum air temperature, 25° F; liquid-
   water content, 0.83 gram per cubic meter.

Lower surface. Icing time, 2 minutes;
section drag coefficient, 0.0177.

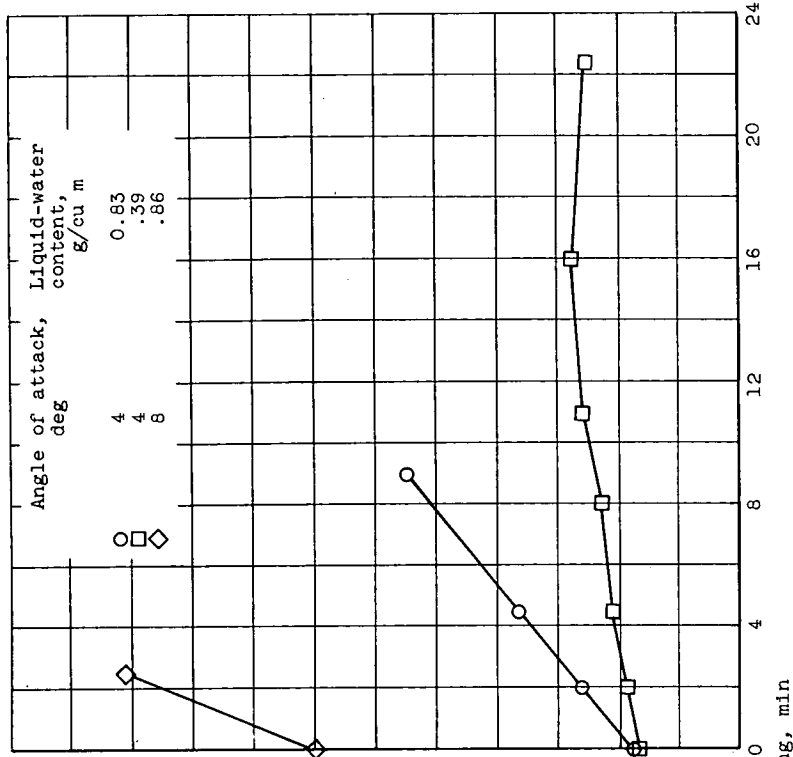Upper surface. Icing time, $2\frac{1}{2}$ minutes;
section drag coefficient, 0.0187.
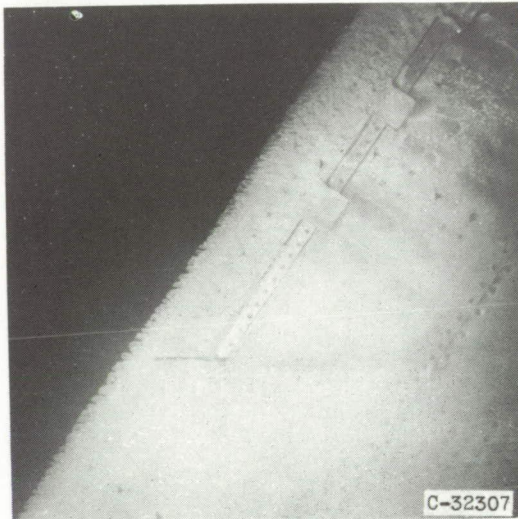
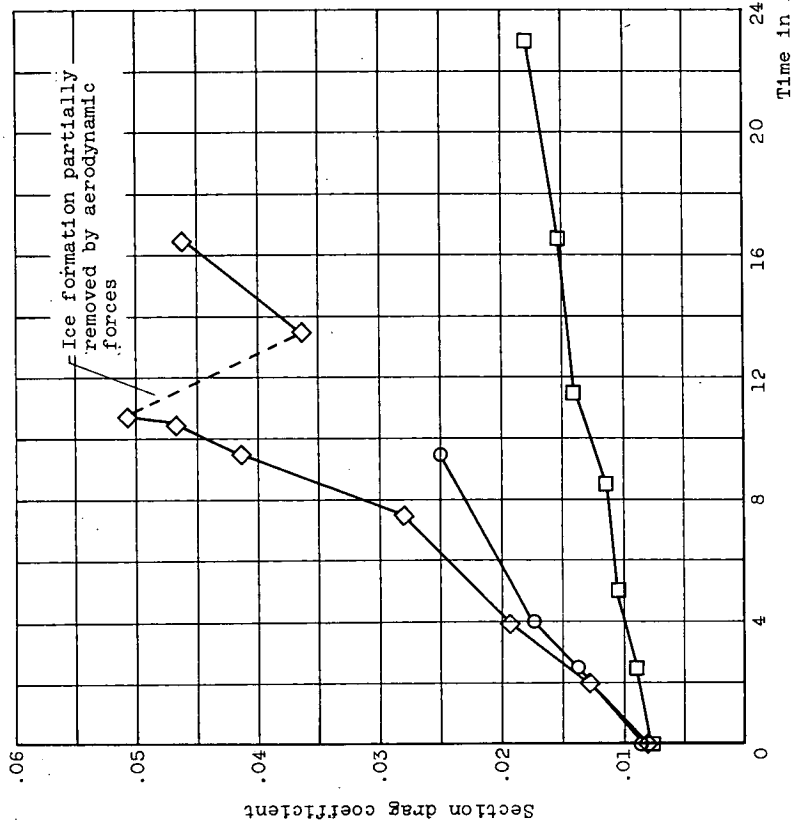Lower surface. Icing time, 5 minutes;
section drag coefficient, 0.0228.

Upper surface. Icing time, $5\frac{1}{2}$ minutes;
section drag coefficient, 0.0239.

(d) Angle of attack, 8°; initial standard-airfoil-section drag
coefficient, 0.0090.

Figure 7. - Continued. Typical glaze-ice formations with high rate of
water catch on unheated airfoil leading-edge section (slat retracted).
Airspeed, 260 miles per hour; datum air temperature, 25° F; liquid-
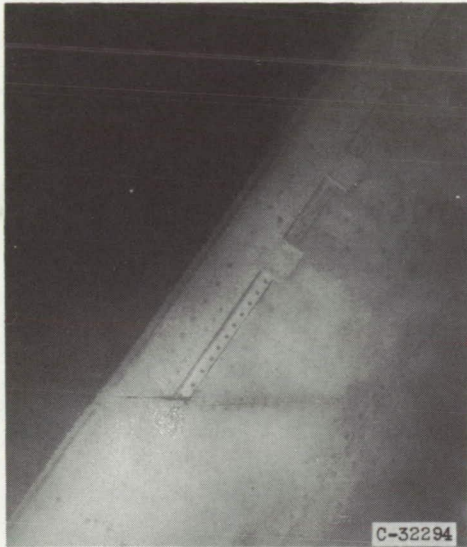water content, 0.83 gram per cubic meter.
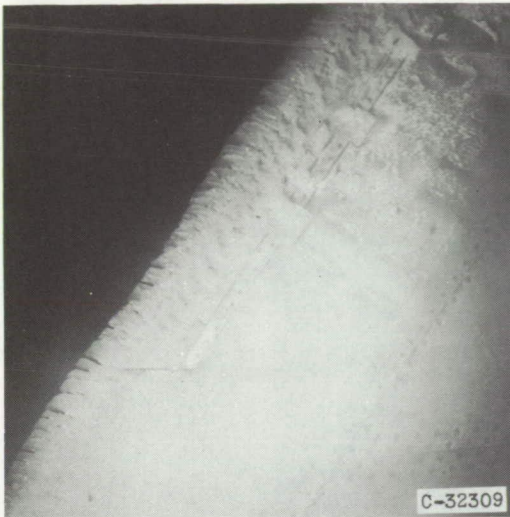
Lower surface. Icing time, $10\frac{1}{2}$ minutes;
section drag coefficient, 0.0350.
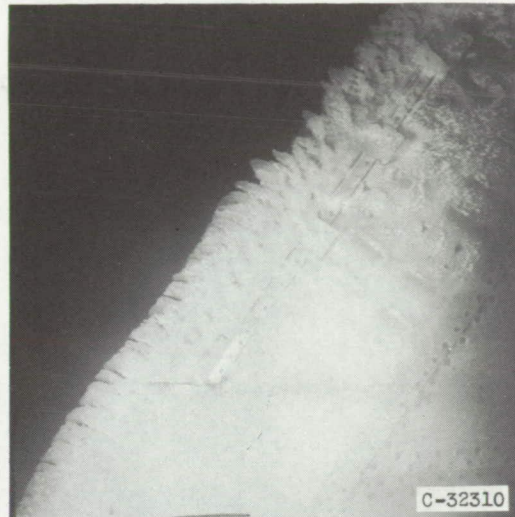
Lower surface. Icing time, 11 minutes;
section drag coefficient, 0.0360.
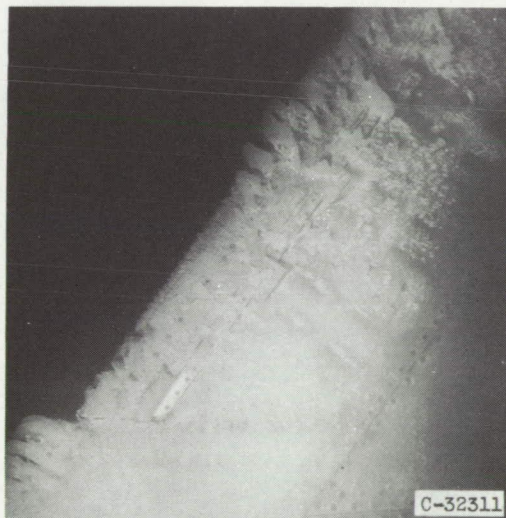
Lower surface. Icing time, 15 minutes;
section drag coefficient, 0.0457.

(d) Concluded. Angle of attack, 8°; initial standard-airfoil-section
    drag coefficient, 0.0090.

Figure 7. - Concluded. Typical glaze-ice formations with high rate of
    water catch on unheated airfoil leading-edge section (slat retracted).
    Airspeed, 260 miles per hour; datum air temperature, 25° F; liquid-
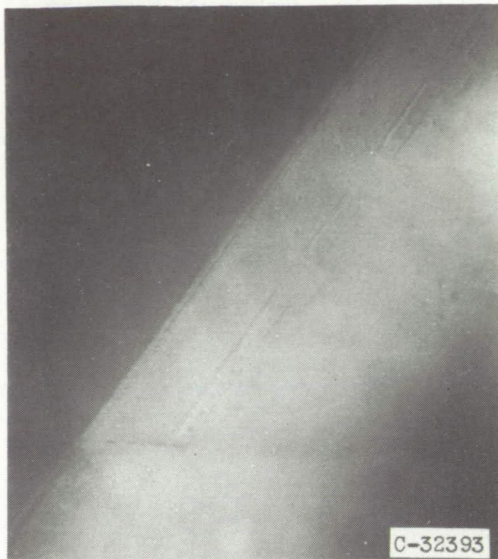   water content, 0.83 gram per cubic meter.
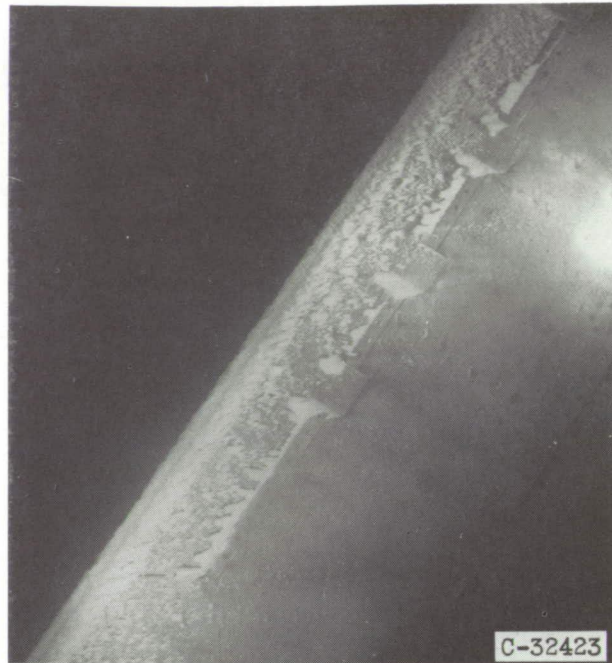
Lower surface. Icing time, $6\frac{1}{2}$ minutes;
section drag coefficient, 0.0160.
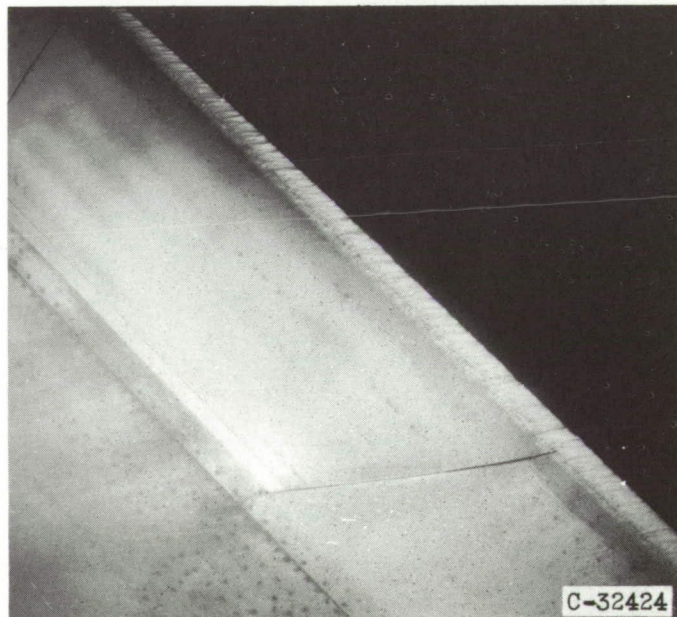
Upper surface. Icing time, $8\frac{1}{2}$ minutes;
section drag coefficient, 0.0172.

Figure 8. - Typical rime-ice formations on unheated airfoil leading-edge
section (slat retracted). Angle of attack, 4°; airspeed, 260 miles
per hour; datum air temperature, 10° F; liquid-water content, 0.55
gram per cubic meter; initial standard-airfoil-section drag coeffi-
cient, 0.0112.

(a) Standard-airfoil section.
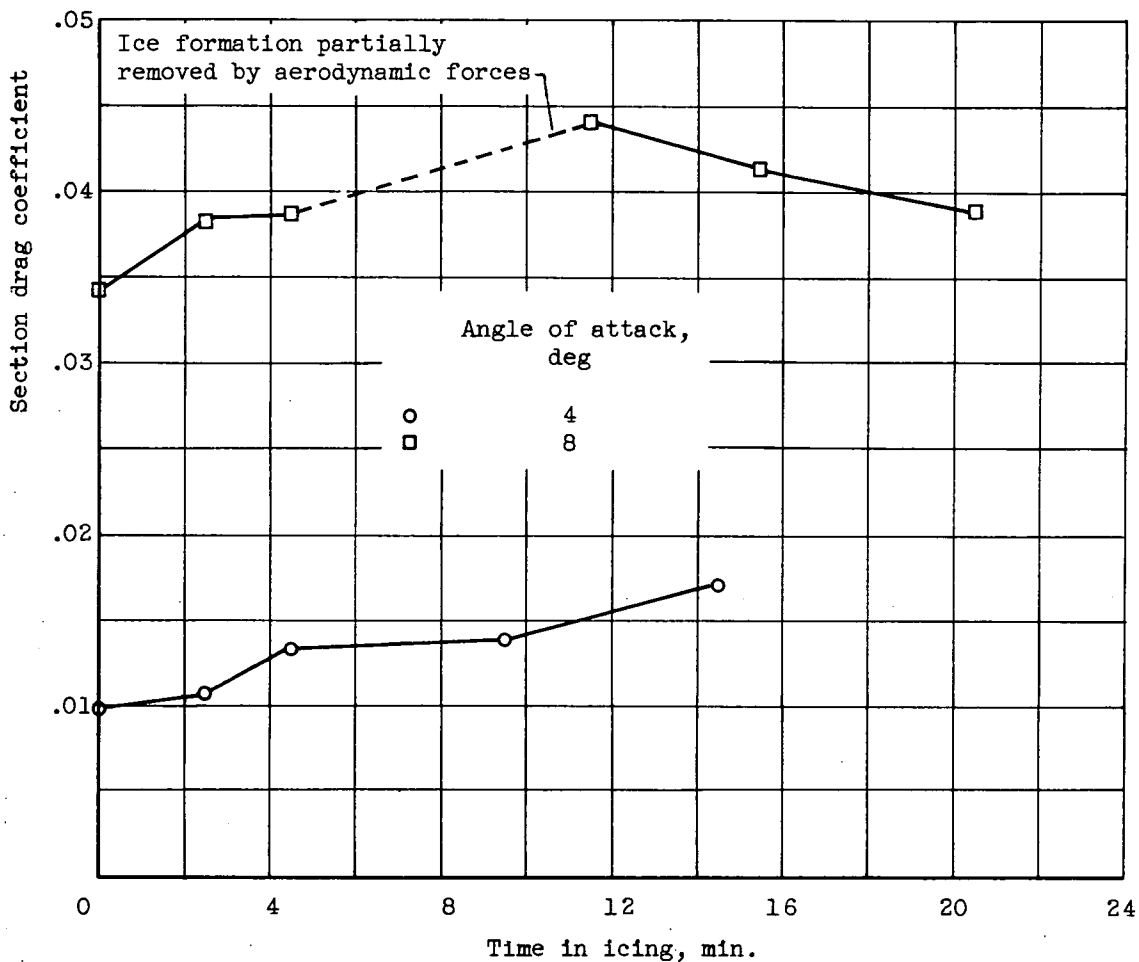
(b) Slatted-airfoil section.

Figure 9. - Variation of section drag coefficient with time in glaze-
icing conditions for unheated airfoil (slat retracted) at a low rate
of water catch. Airspeed, 260 miles per hour; datum air temperature,
25° F; liquid-water content, 0.39 gram per cubic meter.

Lower surface. Icing time, $4\frac{1}{2}$ minutes;
section drag coefficient, 0.0129.

Upper surface. Icing time, 5 minutes;
section drag coefficient, 0.0126.
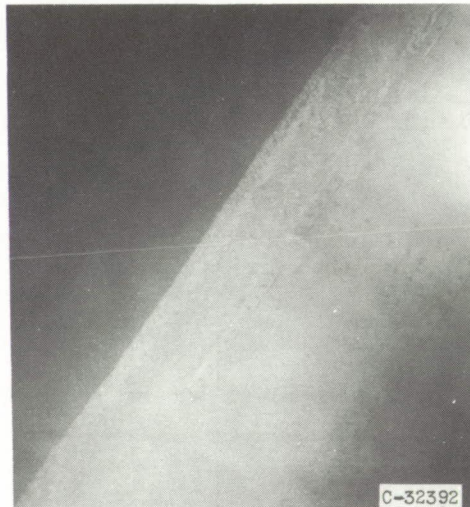
Lower surface. Icing time, $14\frac{1}{2}$ minutes;
section drag coefficient, 0.0179.

(a) Angle of attack, 4°; initial standard-airfoil-section drag
     coefficient, 0.0103.

Figure 10. - Typical glaze-ice formations with low rate of water catch
    on unheated airfoil leading-edge section (slat retracted). Airspeed,
    260 miles per hour; datum air temperature, 25° F; liquid-water con-
    tent, 0.39 gram per cubic meter.

Lower surface. Icing time, 4 minutes;
section drag coefficient, 0.0112.

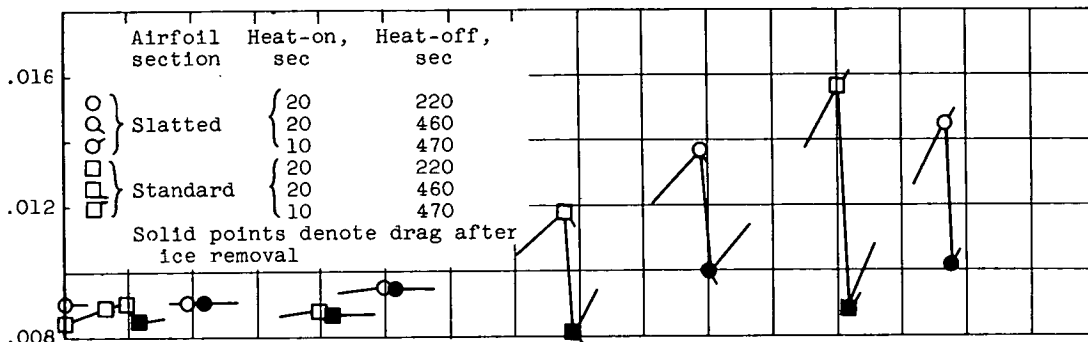Upper surface. Icing time, $4\frac{1}{2}$ minutes;
section drag coefficient, 0.0115.

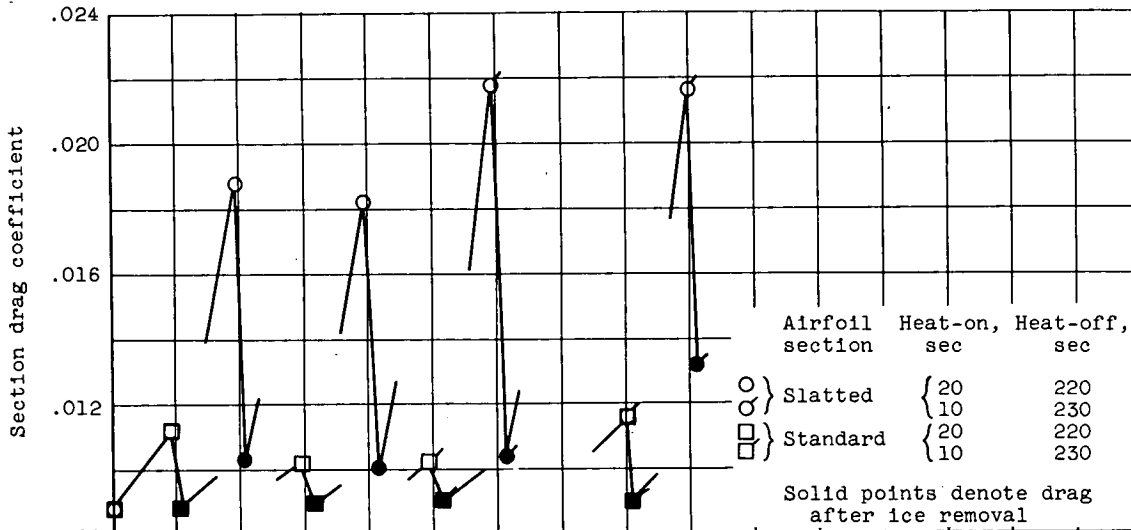Lower surface. Icing time, 10 minutes;
section drag coefficient, 0.0153.

Upper surface. Icing time, 12 minutes;
section drag coefficient, 0.0155.

(b) Angle of attack, 8°; initial standard-airfoil-section drag
     coefficient, 0.0099.

Figure 10. - Concluded. Typical glaze-ice formations with low rate of
    water catch on unheated airfoil leading-edge section (slat retracted).
    Airspeed, 260 miles per hour; datum air temperature, 25° F; liquid-
    water content, 0.39 gram per cubic meter.

(a) Standard-airfoil section.

(b) Slatted-airfoil section.

Figure 11. - Section drag coefficient as function of time in glaze-icing conditions with leading-edge section unheated except for ice-free parting strip (slat retracted). Airspeed, 260 miles per hour; datum air temperature, 25° F.

Lower surface. Icing time, 2 minutes; section drag coefficient, 0.0127.

Lower surface. Icing time, $2\frac{1}{2}$ minutes; section drag coefficient, 0.0136.

Upper surface. Icing time, $4\frac{1}{2}$ minutes; section drag coefficient, 0.0180.

Upper surface. Icing time, 5 minutes; section drag coefficient, 0.0188.

(a) High rate of water catch. Angle of attack, 4°; liquid-water content, 0.83 gram per cubic meter; initial standard-airfoil-section drag coefficient, 0.0085.

Figure 12. - Typical glaze-ice formations on unheated airfoil leading-edge section with ice-free parting strip (slat retracted). Airspeed, 260 miles per hour; datum air temperature, 25° F.

Lower surface. Icing time, $4\frac{1}{2}$ minutes;
section drag coefficient, 0.0101.

Lower surface. Icing time, 11 minutes;
section drag coefficient, 0.0134.
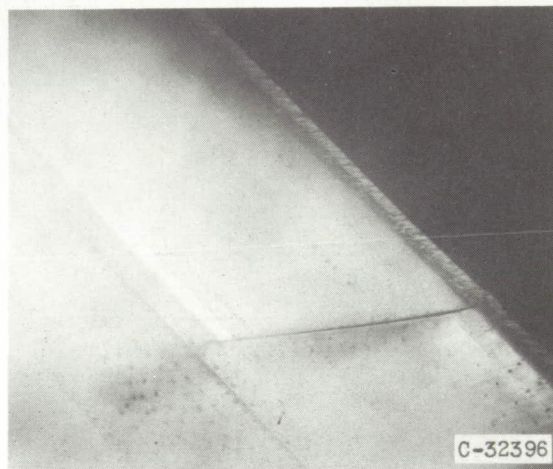
Upper surface. Icing time, $11\frac{1}{2}$ minutes;
section drag coefficient, 0.0140.

(b) Low rate of water catch. Angle of attack, 4°; liquid-water
content, 0.39 gram per cubic meter; initial standard-airfoil-
section drag coefficient, 0.0078.

Figure 12. - Continued. Typical glaze-ice formations on unheated airfoil
leading-edge section with ice-free parting strip (slat retracted). Air-
speed, 260 miles per hour; datum air temperature, 25° F.

Lower surface. Icing time, 4 minutes; section drag coefficient, 0.0192.

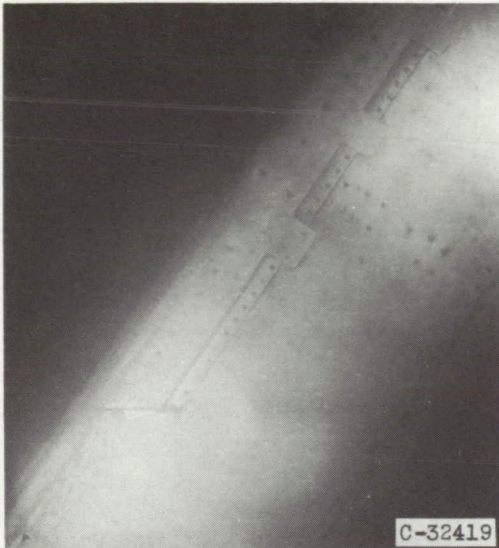Upper surface. Icing time, $7\frac{1}{2}$ minutes; section drag coefficient, 0.0280.

Upper surface. Icing time, $13\frac{1}{2}$ minutes; section drag coefficient, 0.0358.

Lower surface. Icing time, $16\frac{1}{2}$ minutes; section drag coefficient, 0.0461.

(c) High rate of water catch. Angle of attack, 8°; liquid-water content, 0.86 gram per cubic meter; initial standard-airfoil-section drag coefficient, 0.0081.

Figure 12. - Concluded. Typical glaze-ice formations on unheated airfoil leading-edge section with ice-free parting strip (slat retracted). Airspeed, 260 miles per hour; datum air temperature, 25° F.

(a) Angle of attack, 4°; liquid-water content, 0.39 gram per cubic meter.

(b) Angle of attack, 4°; liquid-water content, 0.80 gram per cubic meter.
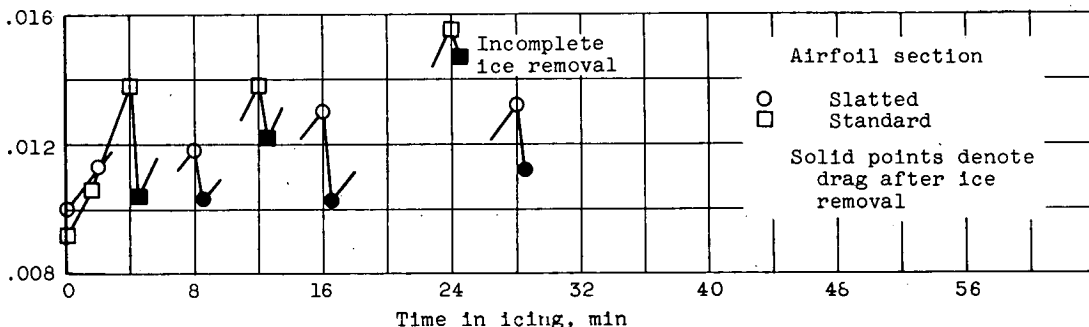
(c) Angle of attack, 2°; liquid-water content, 0.80 gram per cubic meter; icing
period, 220 seconds; heat-on period, 20 seconds.

Figure 13. - Effect of glaze-ice formations on section drag coefficient as func-
tion of time in icing with airfoil leading-edge section cyclically de-iced
(slat retracted). Airspeed, 260 miles per hour; datum air temperature, 25° F.

Lower surface. Icing time, 31 minutes; section drag coefficient, 0.0118; standard airfoil; heat-on period, 20 seconds; heat-off period, 460 seconds.

Upper surface. Icing time, $39\frac{1}{2}$ minutes; section drag coefficient, 0.0136; slatted airfoil; heat-on period, 20 seconds; heat-off period, 460 seconds.

Lower surface. Icing time, 48 minutes; section drag coefficient, 0.0156; standard airfoil; heat-on period, 10 seconds; heat-off period, 470 seconds.

Upper surface. Icing time, $54\frac{1}{2}$ minutes; section drag coefficient, 0.0145; slatted airfoil; heat-on period, 10 seconds; heat-off period, 470 seconds.

(a) Low rate of water catch, before ice removal. Angle of attack, 4°; liquid-water content, 0.39 gram per cubic meter; initial standard-airfoil-section drag coefficient, 0.0085.

Figure 14. - Glaze-ice formations on cyclically de-iced airfoil leading-edge section (slat retracted). Airspeed, 260 miles per hour; datum air temperature, 25° F.
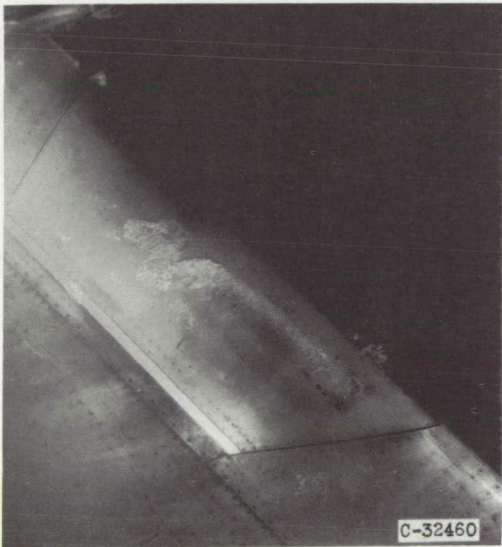
C-32413

C-32411

Lower surface. Icing time, $3\frac{3}{4}$ minutes;
section drag coefficient, 0.0112;
standard airfoil.

Upper surface. Icing time, $7\frac{3}{4}$ minutes;
section drag coefficient, 0.0188;
slatted airfoil.

(b) High rate of water catch, before ice removal. Angle of attack, 4°;
liquid-water content, 0.80 gram per cubic meter; initial standard-
airfoil-section drag coefficient, 0.0088; heat-on period, 20 seconds;
heat-off period, 220 seconds.

Figure 14. - Continued. Glaze-ice formations on cyclically de-iced air-
foil leading-edge section (slat retracted). Airspeed, 260 miles per
hour; datum air temperature, 25° F.

Lower surface. Icing time, 12 minutes;
section drag coefficient, 0.0138; be-
fore ice removal; standard airfoil.

Lower surface. Icing time, $12\frac{1}{2}$ minutes;
section drag coefficient, 0.0122; after
ice removal; standard airfoil.

Upper surface. Icing time, 16 minutes;
section drag coefficient, 0.0130; be-
fore ice removal; slatted airfoil.

(c) High rate of water catch. Angle of attack, 2°; liquid-water con-
tent, 0.80 gram per cubic meter; initial standard-airfoil-section
drag coefficient, 0.0092; heat-on period, 20 seconds; heat-off
period, 220 seconds.

Figure 14. - Concluded. Glaze-ice formations on cyclically de-iced airfoil
leading-edge section (slat retracted). Airspeed, 260 miles per hour;
datum air temperature, 25° F.

(a) Angle of attack, 4°; airspeed, 260 miles per hour; liquid-water content, 0.80 gram per cubic meter.

(b) Angle of attack, 6°; airspeed, 175 miles per hour; liquid-water content, 1.05 grams per cubic meter; standard airfoil section.

(c) Angle of attack, 7°; airspeed, 260 miles per hour; liquid-water content, 0.80 gram per cubic meter.
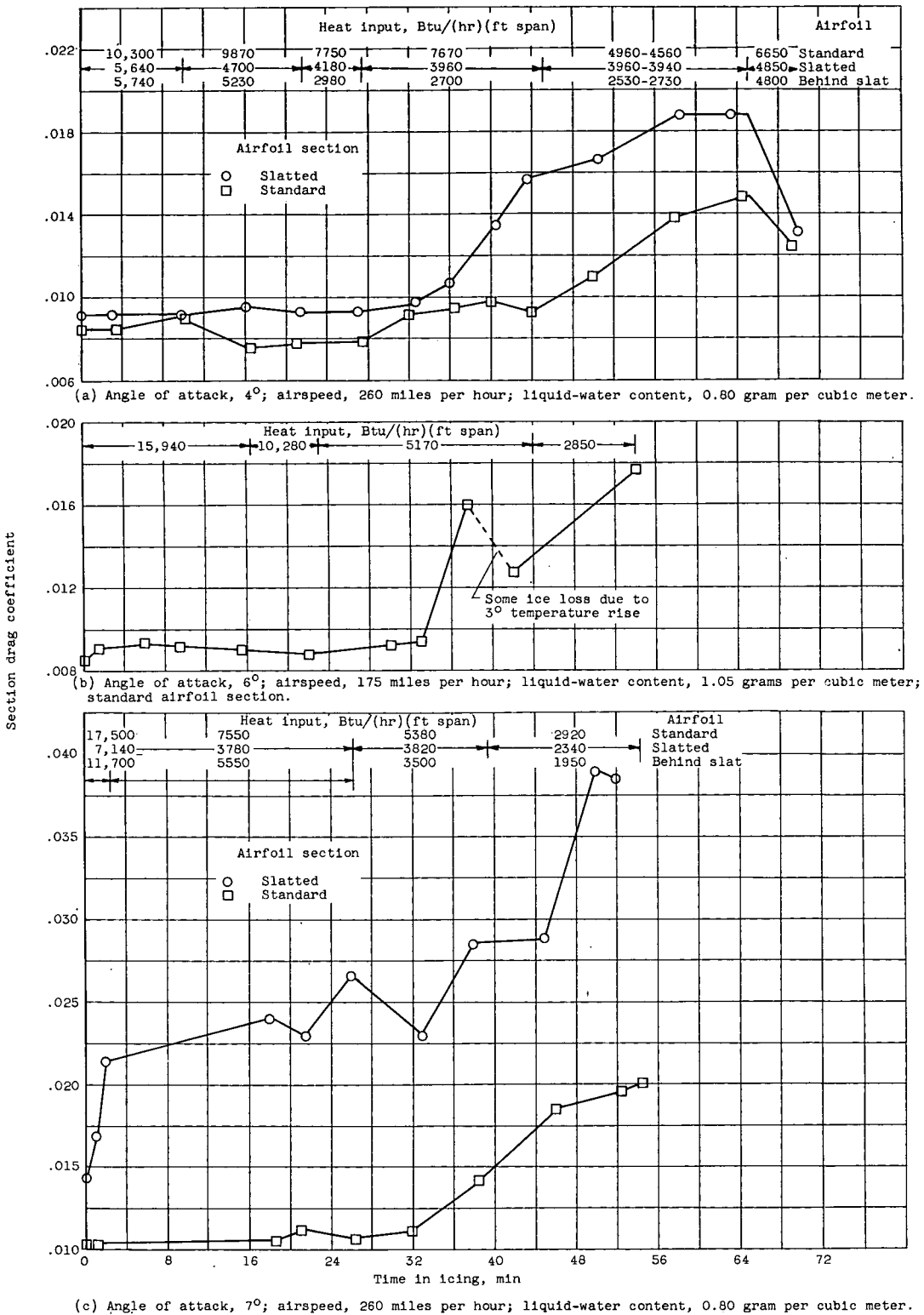
Figure 15. - Effect on section drag coefficient of runback icing incurred with various heating rates as function of time in icing with airfoil leading-edge section continuously heated (slat retracted). Datum air temperature, 25° F.

Upper surface. Icing time, $36\frac{1}{2}$ minutes;
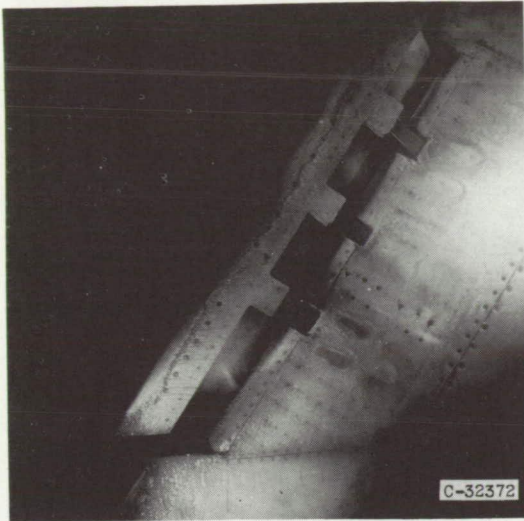section drag coefficient, 0.0095.

Lower surface. Icing time, $43\frac{1}{2}$ minutes;
section drag coefficient, 0.0094.

Upper surface. Icing time, 59 minutes;
section drag coefficient, 0.0140.

Lower surface. Icing time, 64 minutes;
section drag coefficient, 0.0148.

(a) Angle of attack, 4°; initial standard-airfoil-section drag
    coefficient, 0.0085.

Figure 16. - Typical runback icing with high rate of water catch on air-
    foil with continuously heated leading-edge section (slat retracted).
    Airspeed, 260 miles per hour; datum air temperature, 25° F; liquid-
    water content, 0.80 gram per cubic meter.

Upper surface. Icing time, 33 minutes; section drag coefficient, 0.0117.

Lower surface. Icing time, $38\frac{1}{2}$ minutes; section drag coefficient, 0.0142.

Lower surface. Icing time, 46 minutes; section drag coefficient, 0.0185.

Upper surface. Icing time, $50\frac{1}{2}$ minutes; section drag coefficient, 0.0192.

(b) Angle of attack, 7°; initial standard-airfoil-section drag coefficient, 0.0103.

Figure 16. - Concluded. Typical runback icing with high rate of water catch on airfoil with continuously heated leading-edge section (slat retracted). Airspeed, 260 miles per hour; datum air temperature, 25° F; liquid-water content, 0.80 gram per cubic meter.
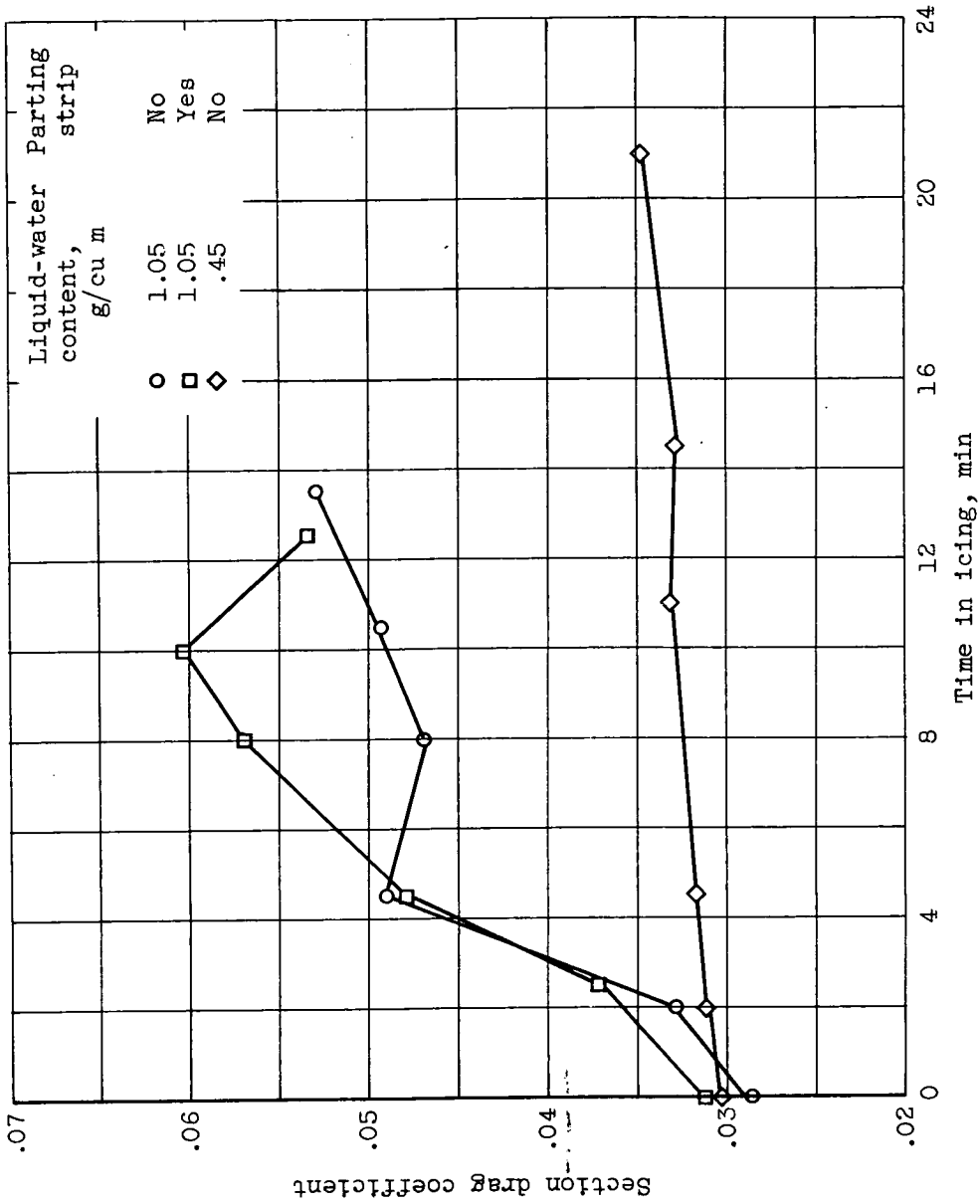
Figure 17. - Variation of section drag coefficient with time in glaze-
icing conditions for unheated airfoil with slat extended halfway.
Slat tracks heated; angle of attack, 6°; airspeed, 175 miles per hour.
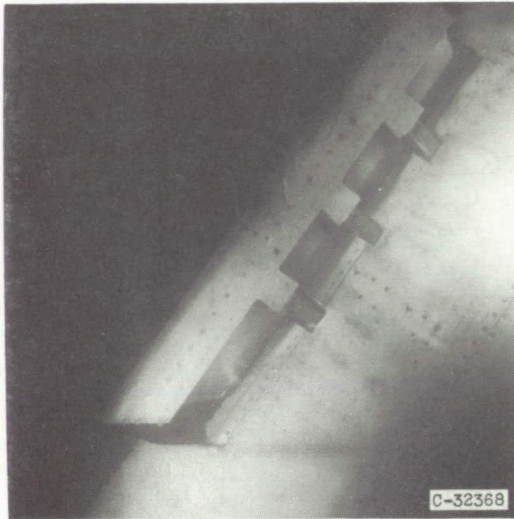
Lower surface. Icing time, 3 minutes; section drag coefficient, 0.0395.

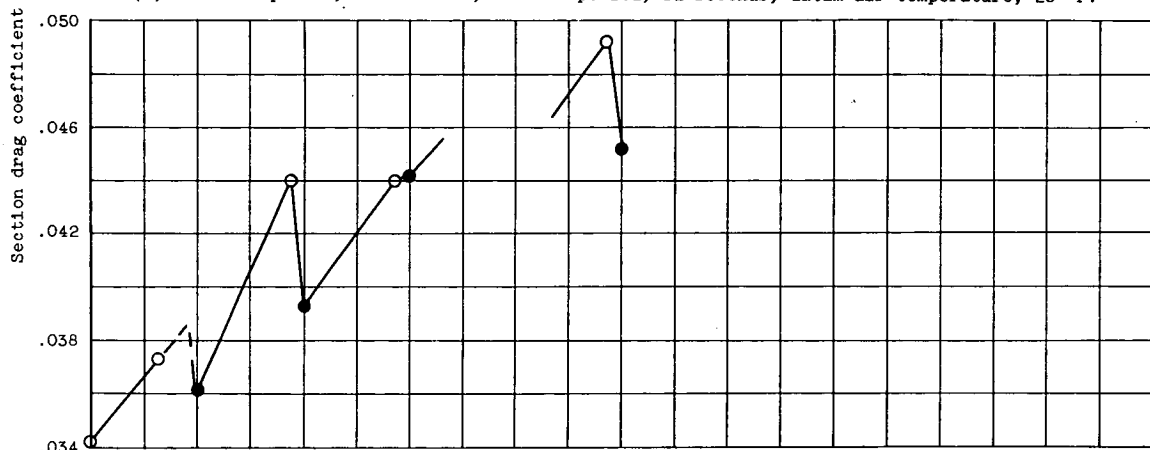Upper surface. Icing time, $5\frac{1}{2}$ minutes; section drag coefficient, 0.0484.

Lower surface. Icing time, $10\frac{1}{2}$ minutes; section drag coefficient, 0.0490.
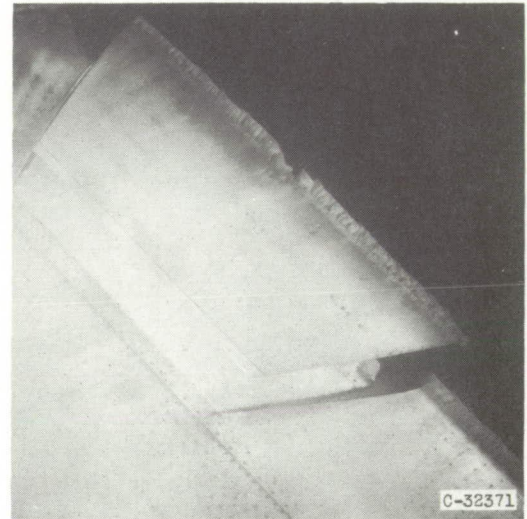
Upper surface. Icing time, 12 minutes; section drag coefficient, 0.0510.

(a) High rate of water catch. Liquid-water content, 1.05 grams per cubic meter; initial section drag coefficient, 0.0286.

Figure 18. - Glaze-ice formations on unheated slatted-airfoil section with slat extended halfway. Angle of attack, 6°; airspeed, 175 miles per hour; datum air temperature, 25° F.

Lower surface.   Icing time, 3 minutes;
section drag coefficient, 0.0398.

Upper surface.   Icing time, 4 minutes;
section drag coefficient, 0.0450.
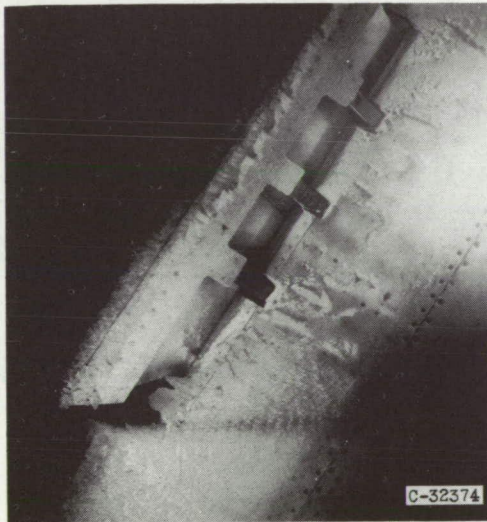
Lower surface.   Icing time, 10 minutes;
section drag coefficient, 0.0602.

Upper surface.   Icing time, 11 minutes;
section drag coefficient, 0.0576.

(b) High rate of water catch; ice-free parting strip. Liquid-water
content, 1.05 grams per cubic meter; initial section drag coeffi-
cient, 0.0312.

Figure 18. - Continued. Glaze-ice formations on unheated slatted-airfoil
section with slat extended halfway. Angle of attack, 6°; airspeed, 175
miles per hour; datum air temperature, 25° F.

Lower surface. Icing time, 4 minutes;
section drag coefficient, 0.0315.

Upper surface. Icing time, 5 minutes;
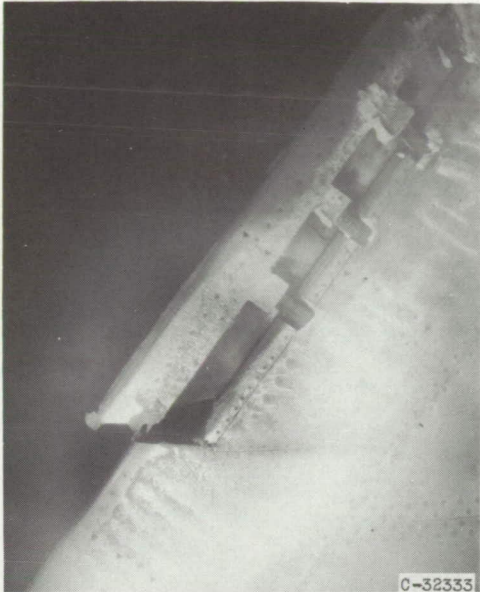section drag coefficient, 0.0317.
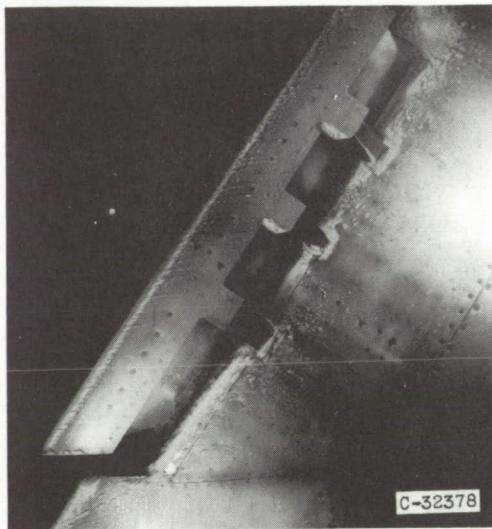
Lower surface. Icing time, 10 minutes;
section drag coefficient, 0.0329.

Upper surface. Icing time, $11\frac{1}{2}$ minutes;
section drag coefficient, 0.0330.

(c) Low rate of water catch. Liquid-water content, 0.45 gram per
cubic meter; initial section drag coefficient, 0.0305.

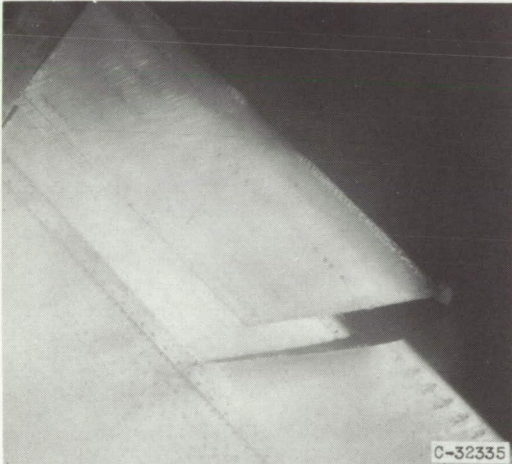Figure 18. - Concluded. Glaze-ice formations on unheated slatted-airfoil
section with slat extended halfway. Angle of attack, 6°; airspeed, 175
miles per hour; datum air temperature, 25° F.
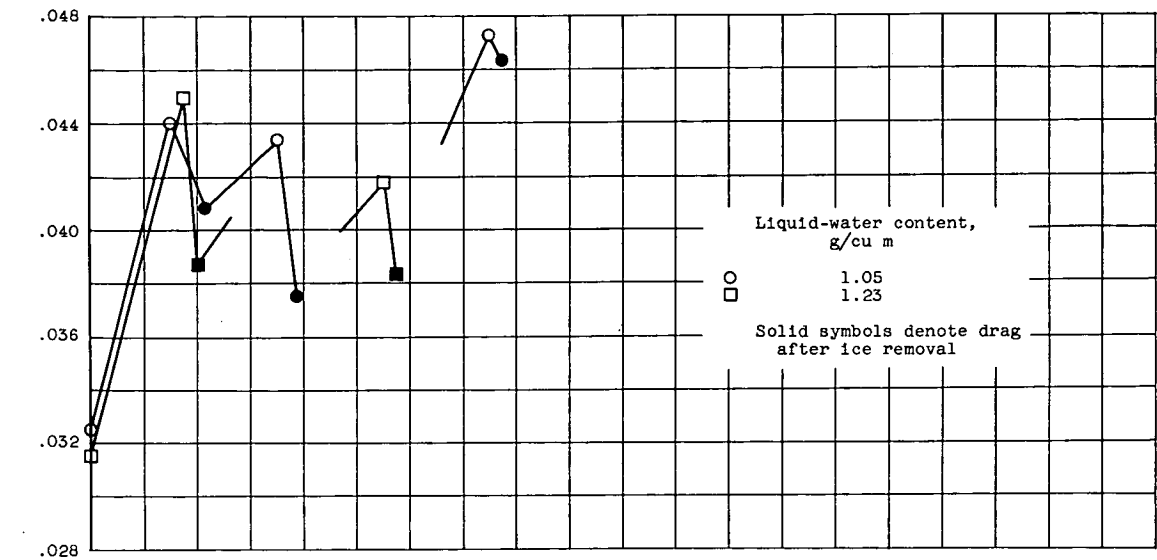
(a) Heat-off period, 220 seconds; heat-on period, 12 seconds; datum air temperature, 25° F.

(b) Liquid-water content, 1.05 grams per cubic meter; heat-off period, 220 seconds; heat-on period, 18 seconds; datum air temperature, 25° F.
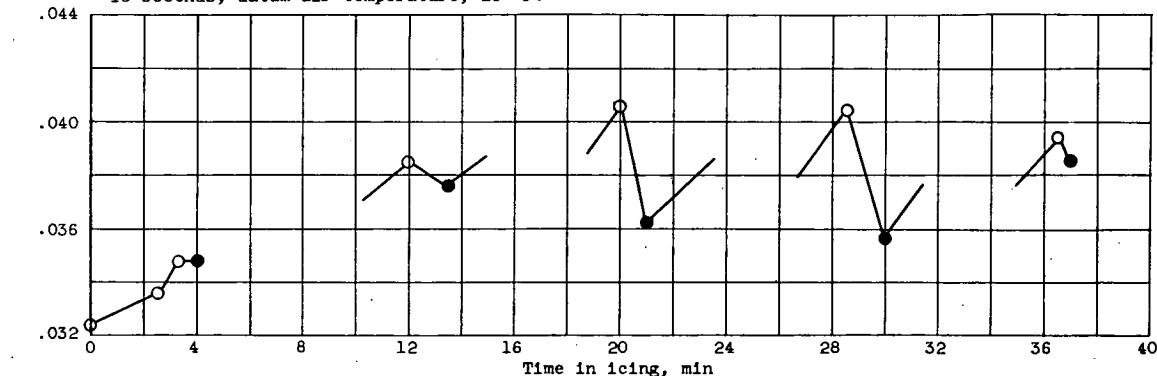
(c) Liquid-water content, 0.64 gram per cubic meter; heat-off period, 220 seconds; heat-on period, 20 seconds; datum air temperature, 10° F.

Figure 19. - Effect of glaze-ice formations on section drag coefficient as function of time in icing with airfoil leading-edge section cyclically de-iced and slat extended halfway. Angle of attack, 6°; airspeed, 175 miles per hour.
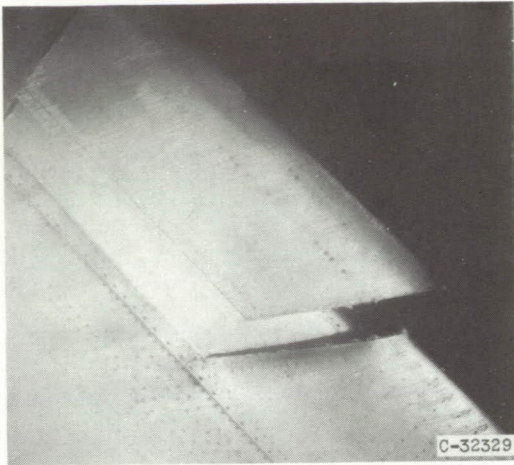
Upper surface. Icing time, 10 minutes;
before ice removal.
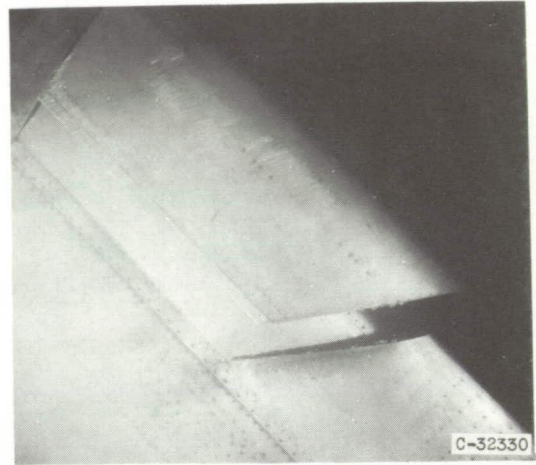
Upper surface. Icing time, $11\frac{1}{2}$ minutes;
after ice removal.
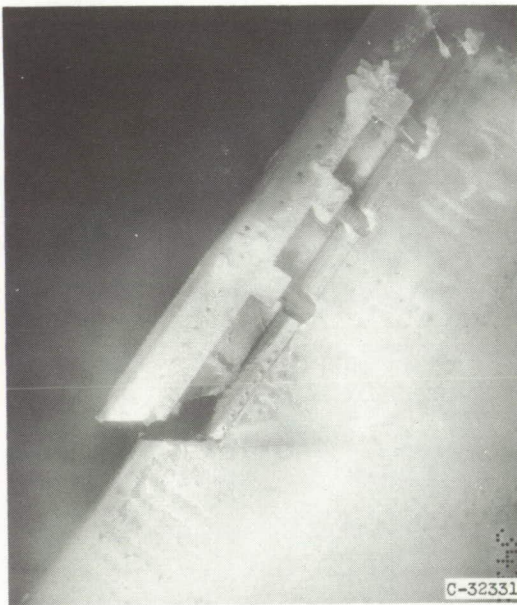
Lower surface. Icing time, 15 minutes;
section drag coefficient, 0.0473; before
ice removal.
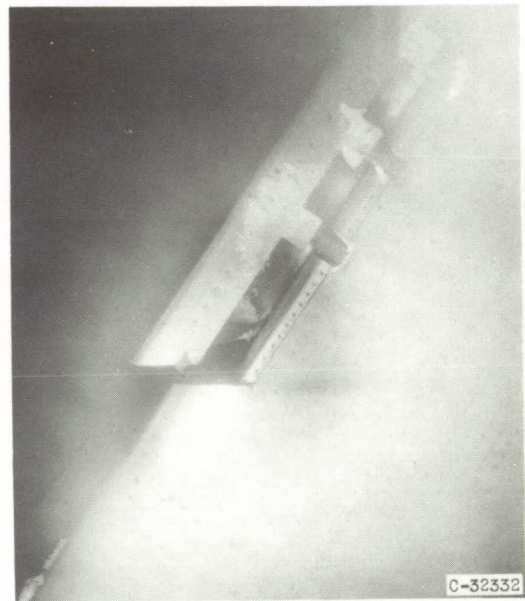
Lower surface. Icing time, $15\frac{1}{2}$ minutes;
section drag coefficient, 0.0463; after
ice removal.

(a) Glaze ice, high rate of water catch. Datum air temperature, 25° F;
     liquid-water content, 1.05 grams per cubic meter; initial section drag
     coefficient, 0.0325; heat-off period, 220 seconds; heat-on period, 12
     seconds.

Figure 20. - Ice formations on cyclically de-iced slatted-airfoil section
     with slat extended halfway. Angle of attack, 6°; airspeed, 175 miles
     per hour.

Lower surface. Icing time, $7\frac{1}{2}$ minutes; before ice removal.
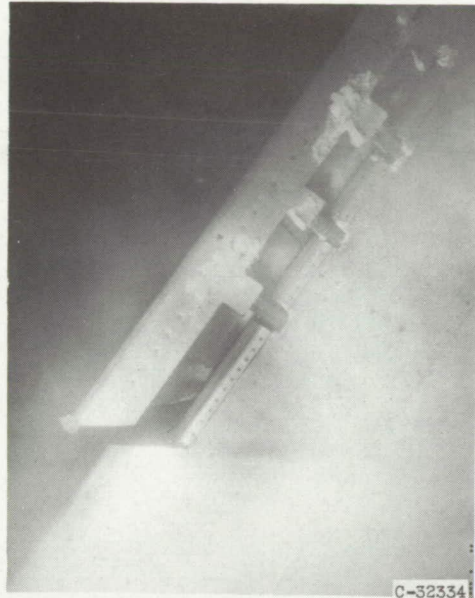
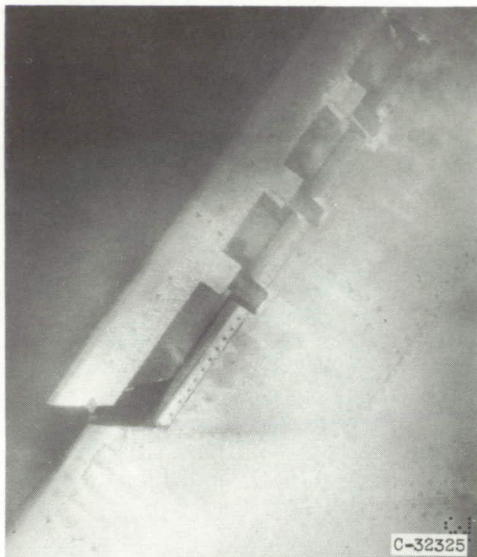Lower surface. Icing time, 8 minutes; after ice removal.

Upper surface. Icing time, 11 minutes; section drag coefficient, 0.0417; before ice removal.
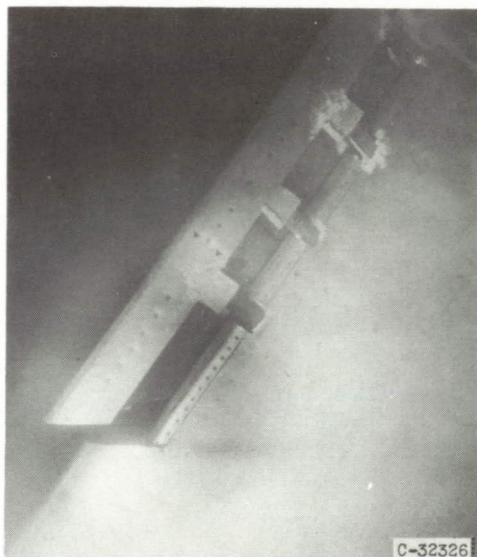

Upper surface. Icing time, $11\frac{1}{2}$ minutes; section drag coefficient, 0.0383; after ice removal.

(b) Glaze ice, high rate of water catch. Datum air temperature, 25° F; liquid-water content, 1.23 grams per cubic meter; initial section drag coefficient, 0.0315; heat-off period, 220 seconds; heat-on period, 12 seconds.

Figure 20. - Continued. Ice formations on cyclically de-iced slatted-airfoil section with slat extended halfway. Angle of attack, 6°; airspeed, 175 miles per hour.

Lower surface. Icing time, $7\frac{1}{2}$ minutes; section drag coefficient, 0.0440; before ice removal.

Lower surface. Icing time, 8 minutes; section drag coefficient, 0.0392; after ice removal.

Upper surface. Icing time, $11\frac{1}{2}$ minutes; section drag coefficient, 0.0440; before ice removal.
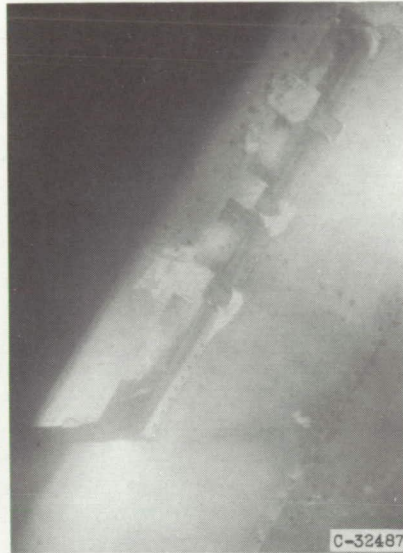

Upper surface. Icing time, 12 minutes; section drag coefficient, 0.0441; after ice removal.

(c) Glaze ice, high rate of water catch. Datum air temperature, 25° F; liquid-water content, 1.05 grams per cubic meter; initial section drag coefficient, 0.0342; heat-off period, 220 seconds; heat-on period, 18 seconds.

Figure 20. - Continued. Ice formations on cyclically de-iced slatted-airfoil section with slat extended halfway. Angle of attack, 6°; airspeed, 175 miles per hour.

Lower surface. Icing time, $32\frac{1}{2}$ minutes; before ice removal.

Lower surface. Icing time, 33 minutes; after ice removal.

Upper surface. Icing time, $36\frac{1}{2}$ minutes; section drag coefficient, 0.0394; before ice removal.

Upper surface. Icing time, 37 minutes; section drag coefficient, 0.0386; after ice removal.

(d) Rime ice. Datum air temperature, 10° F; liquid-water content, 0.64 gram per cubic meter; initial section drag coefficient, 0.0324; heat-off period, 220 seconds; heat-on period, 20 seconds.

Figure 20. - Concluded. Ice formations on cyclically de-iced slatted-airfoil section with slat extended halfway. Angle of attack, 6°; airspeed, 175 miles per hour.
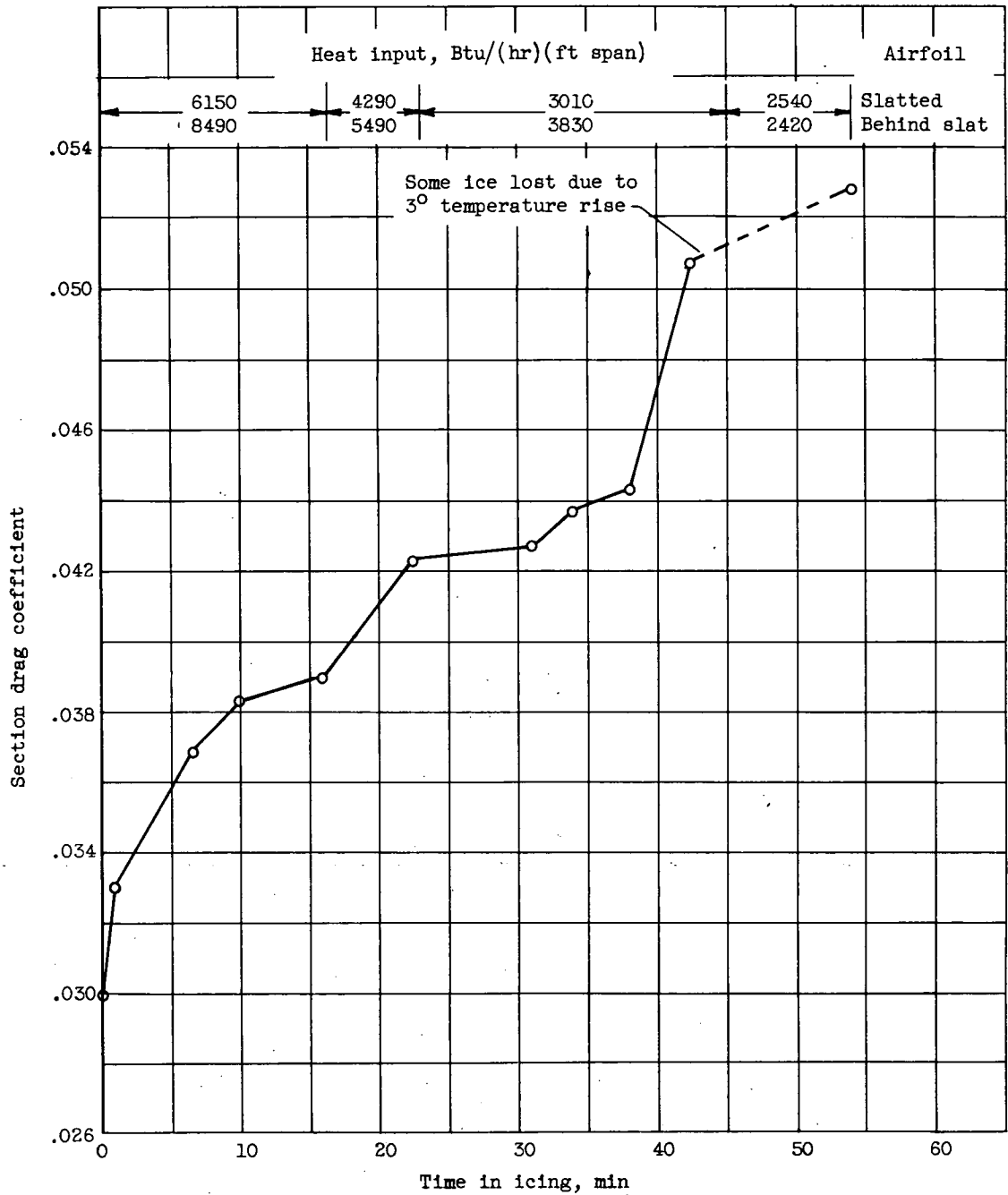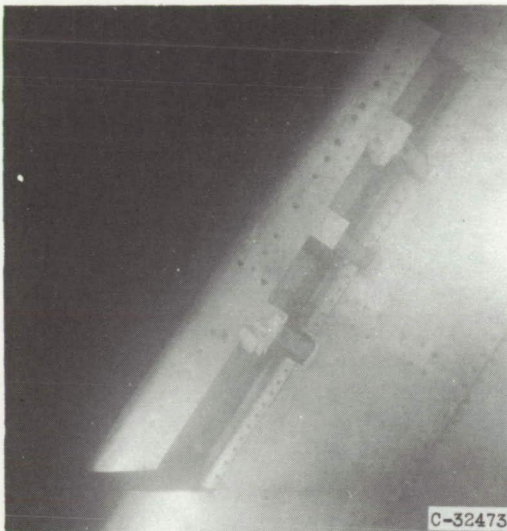
Figure 21. - Effect on section drag coefficient of runback icing incurred with various heating rates as a function of time in icing with airfoil leading-edge section continuously heated and slat extended halfway. Angle of attack, 6°; airspeed, 175 miles per hour; datum air temperature, 25° F; liquid-water content, 1.05 grams per cubic meter.

Lower surface. Icing time, 10 minutes;
section drag coefficient, 0.0383.

Upper surface. Icing time, 13 minutes;
section drag coefficient, 0.0386.

Lower surface. Icing time, 31 minutes;
section drag coefficient, 0.0427.

Upper surface. Icing time, 33 minutes;
section drag coefficient, 0.0434.

Figure 22. - Typical runback ice formations with high rate of water catch
on slatted airfoil with continuously heated leading-edge section and
slat extended halfway. Angle of attack, 6°; airspeed, 175 miles per
hour; datum air temperature, 25° F; liquid-water content, 1.05 grams
per cubic meter; initial section drag coefficient, 0.0299.
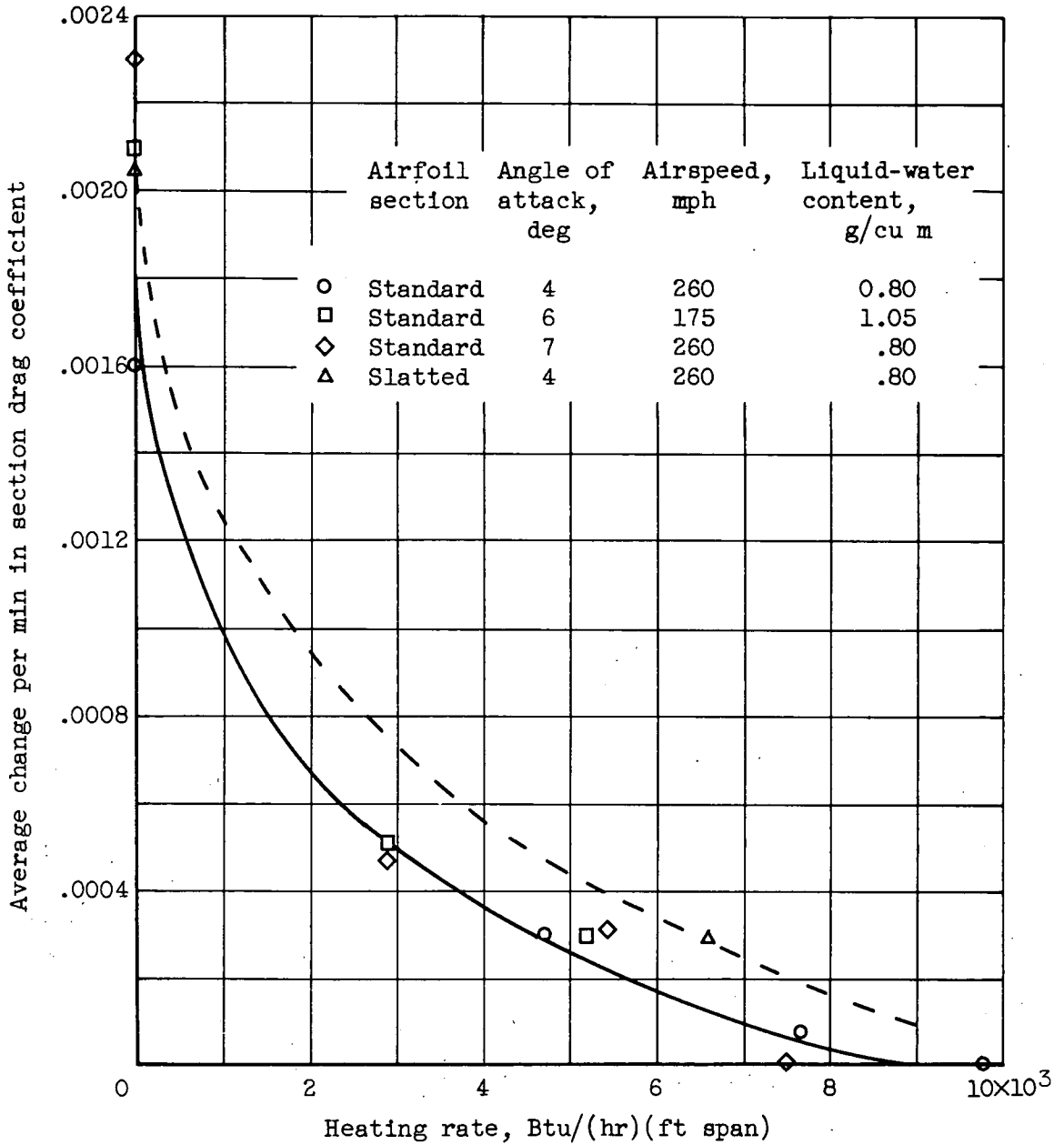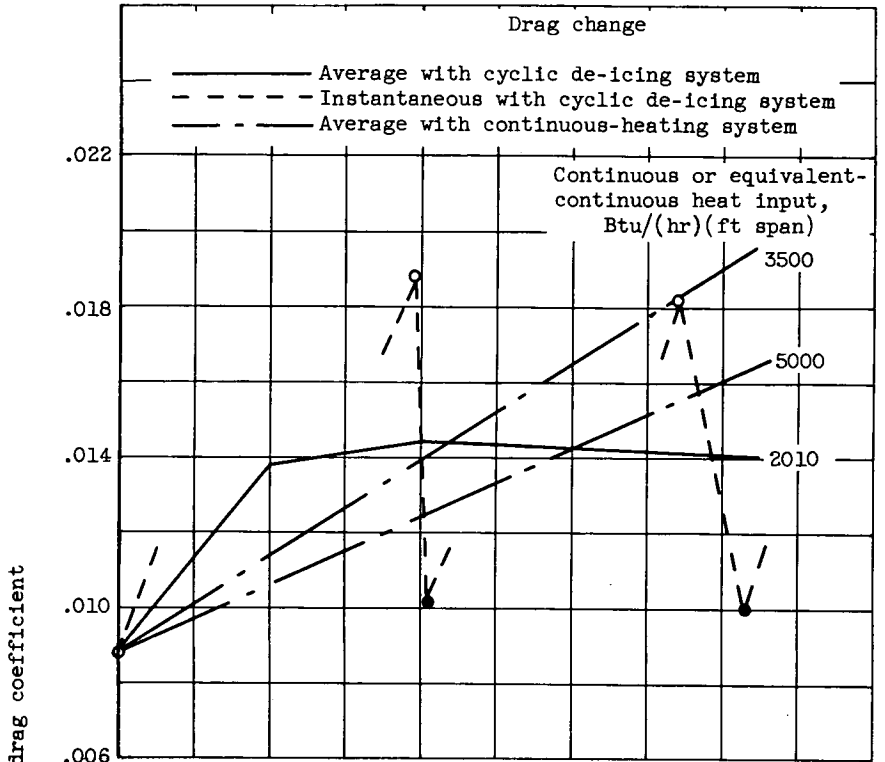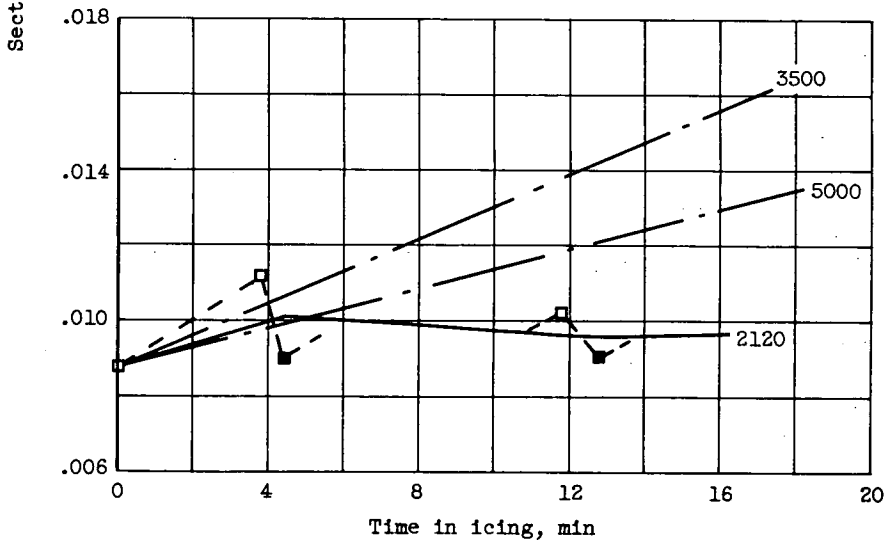
Figure 23. - Average change in section drag coefficient per
    unit of time as function of heating rate for continuously
    heated airfoil leading-edge section (slat retracted).
    Datum air temperature, 25° F.

(a) Slatted-airfoil section (slat retracted).

(b) Standard-airfoil section.

Figure 24. - Comparison of average drag increase in icing
conditions for continuous-heating and cyclic de-icing
systems for several heating rates (slat retracted). Air-
speed, 260 miles per hour; datum air temperature, 25° F;
angle of attack, 4°; liquid-water content, approximately
0.80 gram per cubic meter; heat-on period, 20 seconds;
heat-off period, 220 seconds.